Accurate and Rapid Determination of Fatigue Damage in Bridge Superstructures

Physical Research Report No. 106

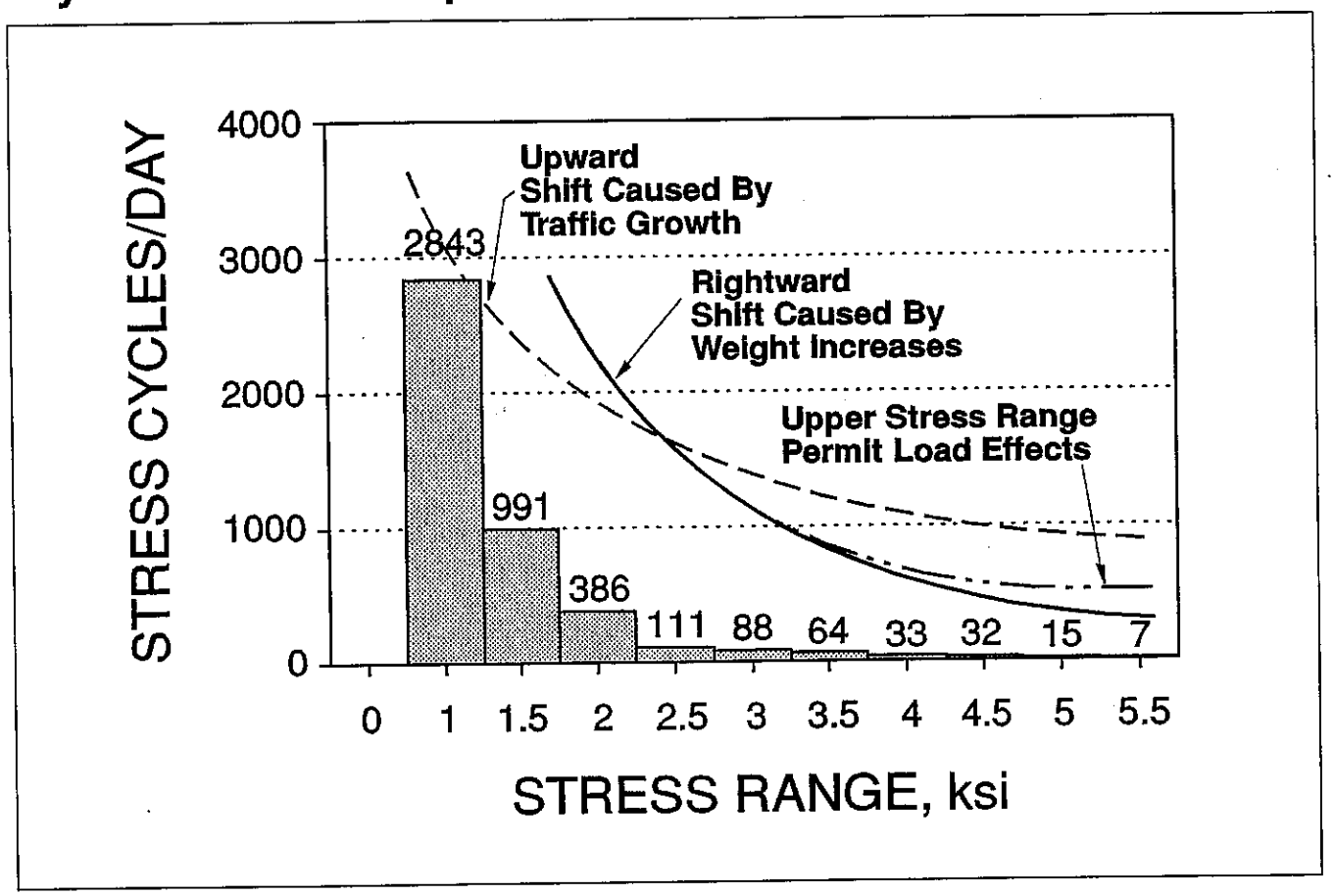

Illinois Department of Transportation

Bureau of Materials and Physical Research

Accurate and Rapid Determination of Fatigue Damage in Bridge Superstructures

Physical Research Report No. 106

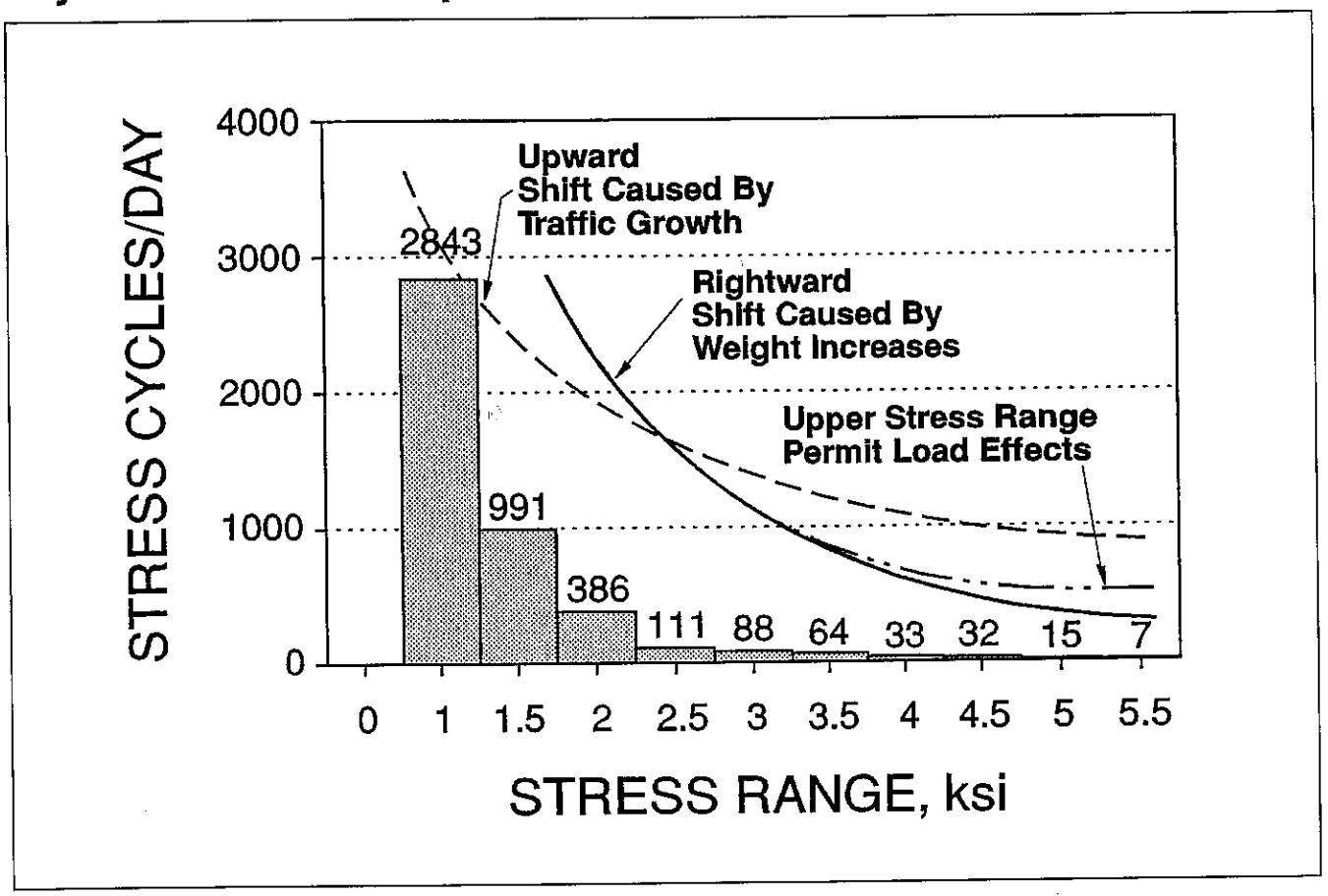

Illinois Department of Transportation

Bureau of Materials and Physical Research

Accurate and Rapid Determination of Fatigue Damage in Bridge Superstructures

Physical Research Report No. 106

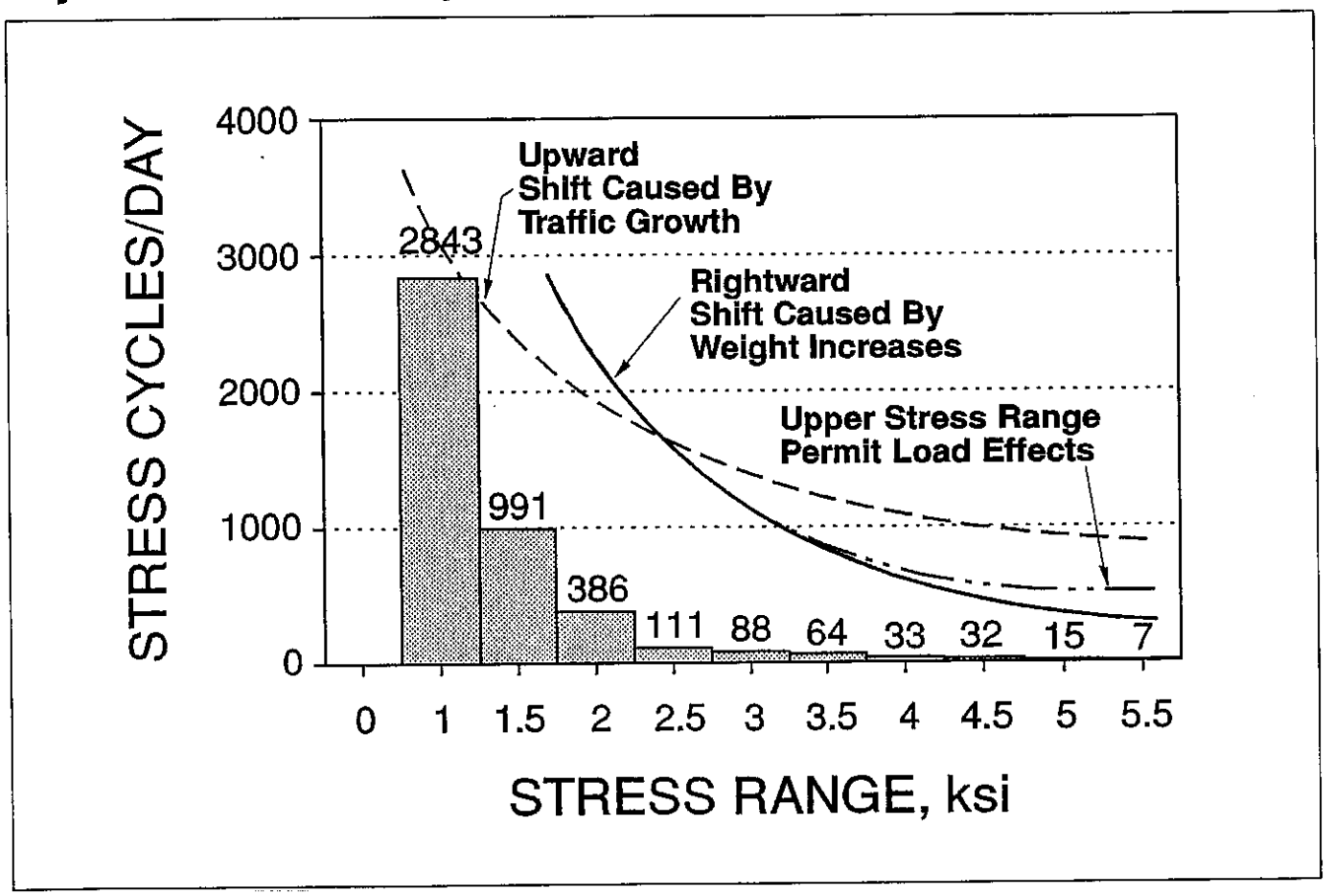

Illinois Department of Transportation

Bureau of Materials and Physical Research

Accurate and Rapid Determination of Fatigue Damage in Bridge Superstructures

Physical Research Report No. 106

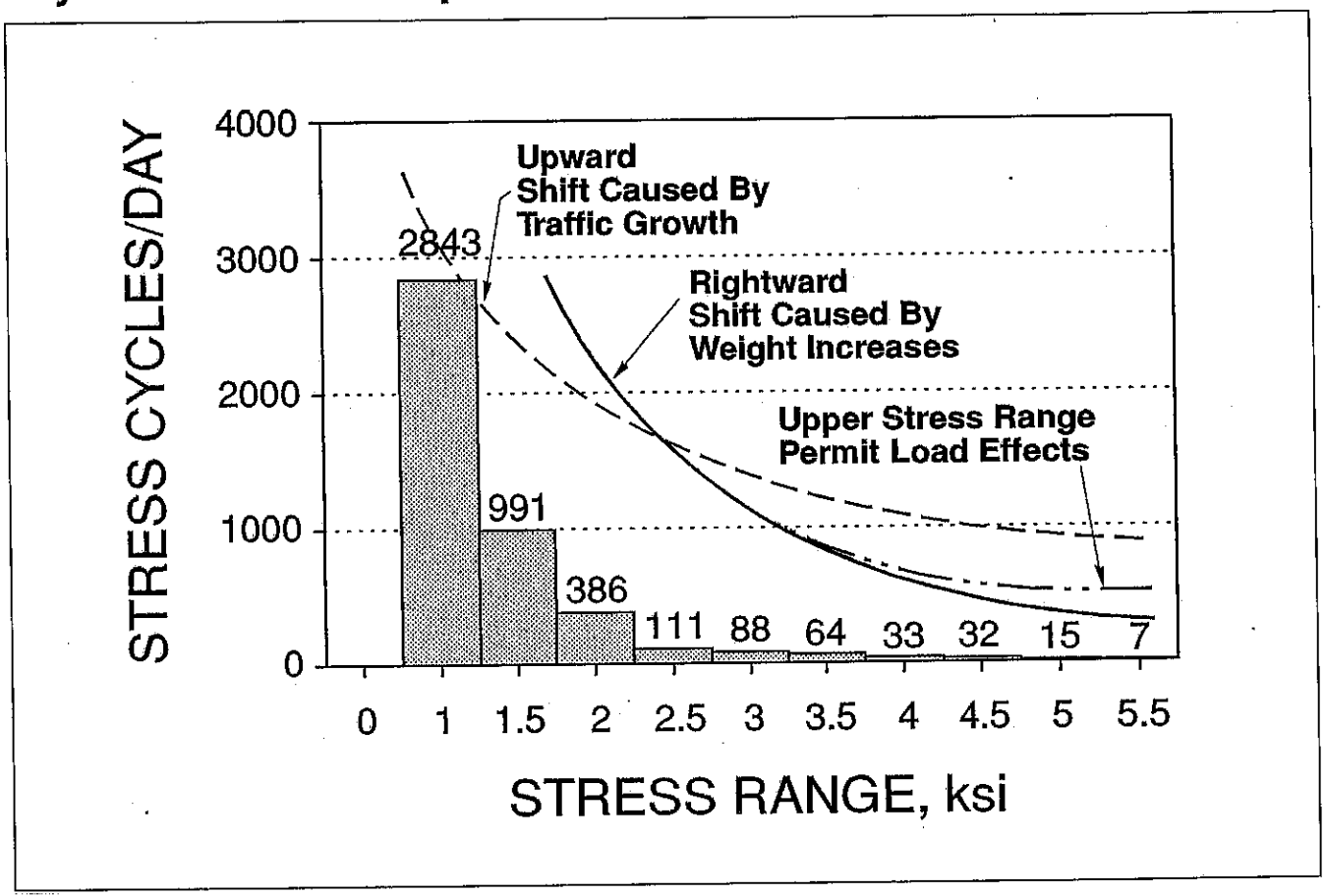

Illinois Department of Transportation

Bureau of Materials and Physical Research

Technical Report Documentation Page

1. Report No.	2. Government Accession No.	3. Recipient's Catalog No.
FHWA/IL/PR-106		

4. Title and Subtitle	5. Report Date
Accurate and Rapid Determination of Fatigue Damage in Bridge Superstructures	December 1992
	6. Performing Organization Code
	8. Performing Organization Report No.
7. Author(s) Christopher Hahin & Jeffrey M. South	PRR-106
9. Performing Orgnization Name and Address Illinois Department of Transportation Bureau of Materials and Physical Research 126 E. Ash Street Springfield, IL 62704-4766	10. Work Unit No. (TRAIS)
	11. Contract or Grant No.
	13. Type of Report and Period Covered Special Report: May 1991 to December 1992
12. Sponsoring Agency Name and Address Illinois Department of Transportation Bureau of Materials and Physical Research 126 E. Ash Street Springfield, IL 62704-4766	14. Sponsoring Agency Code

15. Supplementary Notes

16. Abstract

Fifteen representative steel bridges throughout the State of Illinois were instrumented with foil strain gages to determine their frequencies of loading and the magnitudes of stresses induced by traffic over a 3 to 8-hour period, depending on traffic volume. Reinforced prestressed or post-tensioned concrete bridges were not included in this study. Fatigue prone details, such as cover plated wide flanges, were instrumented. For each stress range increment gathered by the data acquisition system, the cumulative damage sustained over an extended number of years was compared with the number of available fatigue cycles for that stress range using published S-N data for various details and the Palmgren Miner linear damage rule. A new equation for factor of safety for structural details subject to fatigue is described, taking dead load, live load, and bridge detail fatigue strengths into account. A new histogram-linear damage method of assessing future fatigue damage in bridges which takes traffic growth and increased truck weights into account is also described. Other non-welded designs to main load carrying members were examined for susceptibility to fatigue effects, including riveted beams, weathering steels, reinforced concrete in air (without severe cracking), and post-tensioned beams through a review and discussion of the literature. The actual effect of an increase in gross vehicle weight on the measured maximum stress range response of a particular bridge was measured. The histogram-linear damage method favorably compared with the root mean cube-linear damage method and to the fatigue damage procedures given in NCHRP 299.

17. Key Words	18. Distribution Statement
Bridges, fatigue, factor of safety, traffic growth, truck weights, steel cumulative damage, corrosion, deck deterioration, increased truck weight limits.	No restrictions. This document is available to the public through the National Technical Information Service, Springfield, VA 22161

19. Security Classif. (of this report)	20. Security Classif. (of this page)	21. No. of Pages	22. Price
Unclassified	Unclassified	96	

Form DOT F 1700.7 (8-72) Reproduction of completed page authorized

ACCURATE AND RAPID DETERMINATION OF FATIGUE DAMAGE IN BRIDGE SUPERSTRUCTURES

Christopher Hahin, P.E.
Engineer of Bridge Investigations

Jeffrey M. South, P.E.
Structural Analyst

Physical Research Report No. 106
Illinois Department of Transportation
Bureau of Materials and Physical Research

December 1992

FOREWORD

This report should be of interest to engineers involved in bridge design, planning, maintenance and inspection; consultants, and other technical personnel concerned with the life cycles of bridges.

NOTICE

The contents of this report reflect the views of the authors who are responsible for the facts and the accuracy of the data presented herein. The contents do not necessarily reflect the official views or policy of the Federal Highway Administration or the Illinois Department of Transportation. This report does not constitute a standard, specification, or regulation.

Neither the United States Government nor the State of Illinois endorses products or manufacturers. Trade or manufacturers' names appear herein solely because they are considered essential to the object of this report.

ACKNOWLEDGEMENTS

The authors gratefully acknowledge the kind assistance and support of: Professor Jamshid Mohammadi and Professor Sidney Guralnick and their Research Assistant Ramakrishna Polepeddi of the Department of Civil Engineering, Illinois Institute of Technology; Mr. John Rohrer, Chief of Structural Services (retired), Bureau of Bridges and Structures; Mr. James G. Gehler, Chief Engineer, Materials and Research, and Mr. Eric Harm, Engineer of Physical Research, Bureau of Materials and Physical Research, Illinois Department of Transportation. This report represents the complete record of the experimental and theoretical studies performed by the authors that are summarized in a paper scheduled for January 1993 publication in the ASCE Journal of Structural Engineering.

DEDICATION

This report is dedicated to the memory of Mr. Floyd K. Jacobsen, P.E., who made many substantial contributions to bridge technology as Engineer of Bridge Investigations during his lifetime while working for the Illinois Department of Transportation.

TABLE OF CONTENTS

LIST OF FIGURES

LIST OF FIGURES (CONT'D.)

LIST OF FIGURES (CONT'D.)

LIST OF FIGURES (CONT'D.)

LIST OF TABLES

LIST OF ABBREVIATIONS

AASHTO	=	American Association of State Highway and Transportation Officials
ADT	=	average daily traffic
ASTM	=	American Society for Testing and Materials
AWS	=	American Welding Society
DOD	=	Department of Defense
Hz	=	Hertz (SI unit for cycles per second)
I-(X)	=	Interstate Route
NCHRP	=	National Cooperative Highway Research Program
S - N	=	stress range vs. no. of stress cycles
SAE	=	Society of Automotive Engineers
UTS	=	ultimate tensile strength
YS	=	yield strength

1. INTRODUCTION

A vital need exists to rapidly and accurately determine the amount of fatigue damage sustained by bridge superstructures by direct measurement of their actual traffic patterns and the true stresses registered in their main load-carrying members. Prior approaches are largely indirect, analytical methods which determine the stresses in various sections by static analysis using design dead loads and anticipated live loads. The stresses obtained by analytical methods are then compared with the allowable stresses of the AASHTO[1] or other bridge design codes[2] to assure that particular details susceptible to damage have an adequate fatigue life. Methods to assess fatigue damage in steel superstructures are well developed, whereas methods for prestressed reinforced concrete and post-tensioned concrete members are much more limited. In addition, a rational method of calculating a factor of safety consistent with accepted fatigue practice and existing structural codes is also needed.

The Transportation Research Board of the National Research Council has proposed three indirect analytical methods in NCHRP Report 299, Fatigue Evaluation Procedures for Steel Bridges.[3] Each of these methods described in Appendices A, B, and C of NCHRP 299 share a basic form of the equation for remaining fatigue life:

$$Y = \frac{f\,[K \times 10^6]}{T\,[C][S_r]^3},\ \text{yrs.} \qquad (1)$$

where: Y = desired or remaining life

f = coefficient of safety

K = detail constant, relating its susceptibility to fatigue damage

T = volume of truck traffic, units/day

S_r = stress range under various live loadings, ksi

C = number of stress cycles per truck passage

Unfortunately, these indirect analytical methods rely on estimates of traffic volume and have safety coefficients of wide variation. Since fatigue data also show wide variations, inspections of bridges with severely degraded decks often reveal no apparent visual or overt fatigue damage to the superstructure.

The methods developed in this study were intended to increase the reliability of the assessment of fatigue damage by measuring actual stresses, quantifying damage, and providing a method for calculating a meaningful safety factor which is based on known metallic fatigue failure equations and published stress vs cycles-to-failure (S-N) data for certain structural details. The study included the sampling of stresses from strain gages mounted on actual bridge details over a 3- to 8-hour period. The sampling period depended on traffic volume. Such direct measurements determine actual traffic-induced stresses and take load-sharing and redundancy into account, whereas indirect analytical calculations do not always reflect an accurate state of stress in load-carrying members and structural connections.

Recent increases in allowable gross vehicle weights have resulted in some uncertainty as to the increased fatigue susceptibility of bridges to weight increases. The methods developed in this study provide a means to answer the question of increased fatigue damage.

2. INSTRUMENTATION AND STRAIN GAGES

The strain sensors used in this study were weldable, uniaxial foil strain gages (MicroMeasurements of Raleigh, North Carolina). These weldable strain gages consist of a foil gage mounted onto a thin steel shim, which is then micro-spot welded to the detail of interest.

Completion of the Wheatstone bridge circuit was accomplished by using three additional gages mounted on a steel plate which were placed in the vicinity of the active gage. Two to four active gages were typically monitored on each structure.

The strain gages were installed at or close to the steel detail assumed to be the most fatigue-critical in each bridge. On simple spans, this was either at the mid-point of the bridge, or at a flange thickness transition butt weld, or on the link near the pin in a pin-link eyebar connection. On continuous spans, the instrumented detail was at the end of a cover plate.

With the exception of pin-link eyebar connections, all gages were micro-spot welded to the bottom of the lower flange in its thinnest section.

In most instances, strain gages were installed on adjacent beam lines. In this way, both the inner and outer wheel paths, at least in a particular lane, were instrumented.

The data was collected by monitoring general mixed traffic using single channel, microprocessor-based data acquisition equipment manufactured by DataMyte Corporation of Minnetonka, Minnesota, in a data collection format known as "Rainflow." This cycle counting algorithm is described in ASTM E1049-85. Similar data acquisition equipment is available from other manufacturers. Data collection continued for 3 to 8 hours and the resulting stress range histogram was linearly extrapolated

to represent a 24-hour period. The stress range histogram was divided into 0.5 ksi increments, beginning with a value of 1.0 ksi. The Datamyte instrumentation segregates stresses into 0.5 ksi increments and discards all signals from collection with values less than 0.5 ksi because they may include spurious electrical noise.

Although the data sampling period used in this study was less than 24 hours, it does not diminish the methodology established in this report which relies on a 24-hour histogram. Ideally, continuous monitoring of traffic for one week would more properly represent the variation of the number of commuting and commercial vehicles traversing any bridge under study. To account for seasonal changes in loading and frequency, particularly for rural bridges, traffic should be sampled at least for one week several times throughout the year to obtain a better approximation of the true number of fatigue events.

3. SELECTION OF REPRESENTATIVE BRIDGES

The bridges selected were reasonably representative of rural, urban, and interstate routes throughout the State of Illinois. Bridges selected reflected an entire range of truck traffic volume, from as low as 125 trucks/day to 15,800 trucks/day. The study concentrated primarily on older, existing bridges with a heavy emphasis on welded cover-plated girders, which are one of the most fatigue susceptible details (AWS/ AASHTO Category E). The two types of steel bridges instrumented were simple and continuous steel superstructures. Bridges with concrete superstructures were not instrumented. Tables 1, 2, and 3 provide information regarding the distribution of type, nature of traffic, location in the State by District and the surrounding environment.

Figures 1 through 3 show typical illustrative histograms for various traffic spectra, including different traffic volumes and locations. Figure 1 (Bridge 0600126) represents a stress-frequency distribution limited to 1.5 ksi, which is a typical case for bridges primarily conveying passenger cars and light trucks. Figure 2 represents an interstate route, I-80 near Joliet, Illinois, carrying a full array of vehicles (Bridge 0990055). Figure 3 represents a congested urban route near O'Hare airport carrying passenger cars, light and heavy trucks, and various other commercial vehicles (Bridge 0160335). Average histograms and descriptions for each bridge instrumented in this study are shown in Figures 4 through 18. These average histograms were constructed by combining data at each stress range increment derived from data outputs of each active strain gage and then calculating the average value for each increment. A composite stress-frequency diagram was constructed for the State of Illinois based on this representative sample of 15 bridges. Average data for each of the 15 bridges were combined and averaged for

each 0.5 ksi increment to obtain a grand mean, resulting in a composite, representative stress range-frequency histogram for Illinois bridges. This composite histogram is plotted in Figure 19. A complete summary of mean data is shown in Table 4.

TABLE 1

DISTRIBUTION OF INSTRUMENTED BRIDGE TYPES AND TRAFFIC CHARACTERISTICS (COMMERCIAL ADT)

	SIMPLE	CONTINUOUS
HIGH (GREATER THAN 1000)	3	2
MEDIUM (600-1000)	4	2
LOW (LESS THAN 600)	0	4
TOTAL	7	8

TABLE 2

DISTRIBUTION OF BRIDGE TYPE THROUGHOUT ILLINOIS

DISTRICT	SIMPLE	CONTINUOUS
1	3	1
2	2	1
3	2	1
4	0	1
5	0	0
6	0	2
7	0	0
8	0	2
9	0	0
TOTAL	7	8

TABLE 3

DISTRIBUTION OF RURAL VERSUS URBAN ENVIRONMENTS

DISTRICT	URBAN	RURAL
1	4	0
2	2	1
3	2	1
4	0	1
5	0	0
6	0	2
7	0	0
8	0	2
9	0	0
TOTAL	8	7

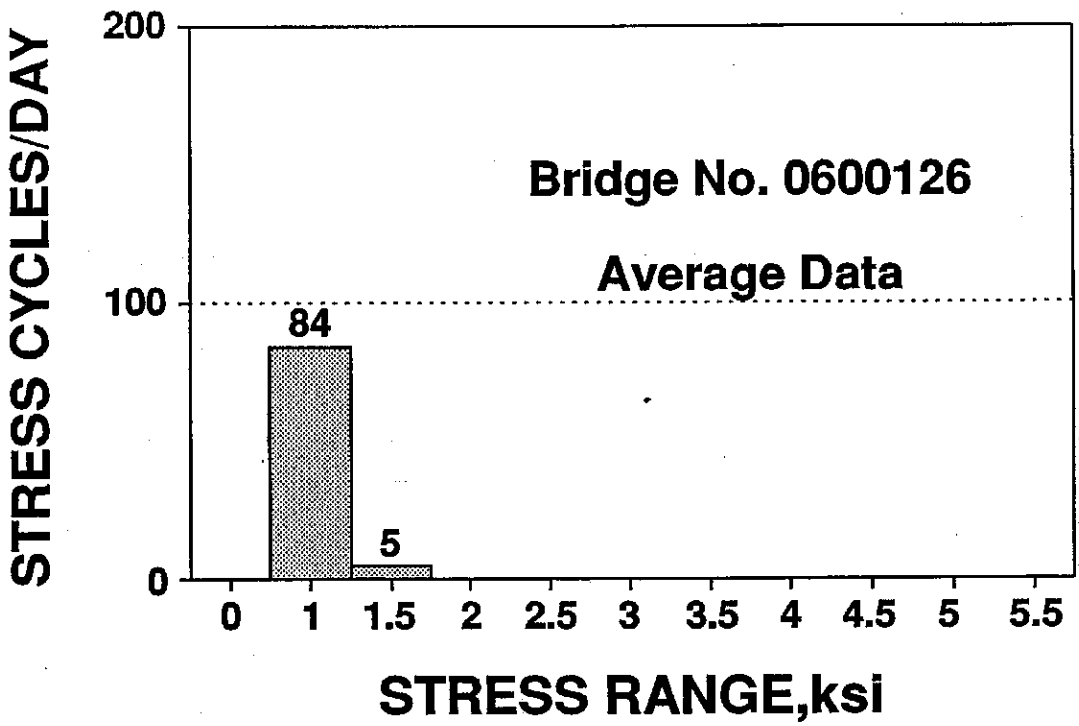

Figure 1. Stress-range vs. frequency histogram for the northbound traffic of IL-111 over the Cahokia Canal near Fairmont City, primarily carrying passenger cars and lighter trucks.

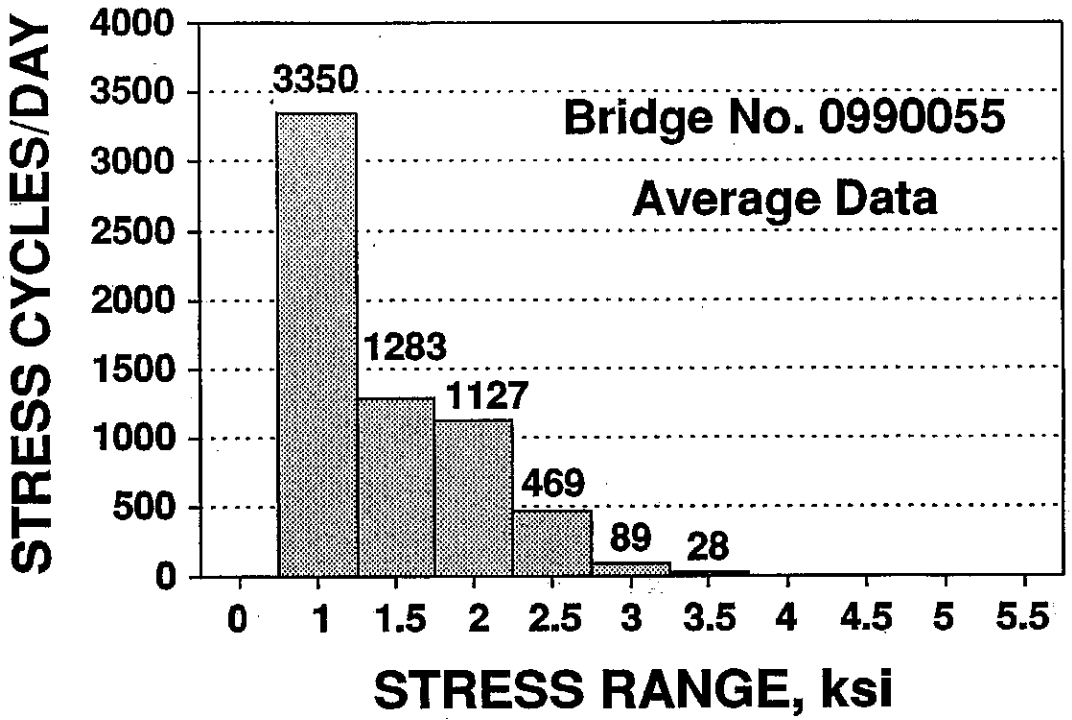

Figure 2. The stress-range vs. frequency diagram for a major suburban interstate highway, I-80 in the westbound direction in Joliet (south of Chicago), carrying a full spectrum of traffic.

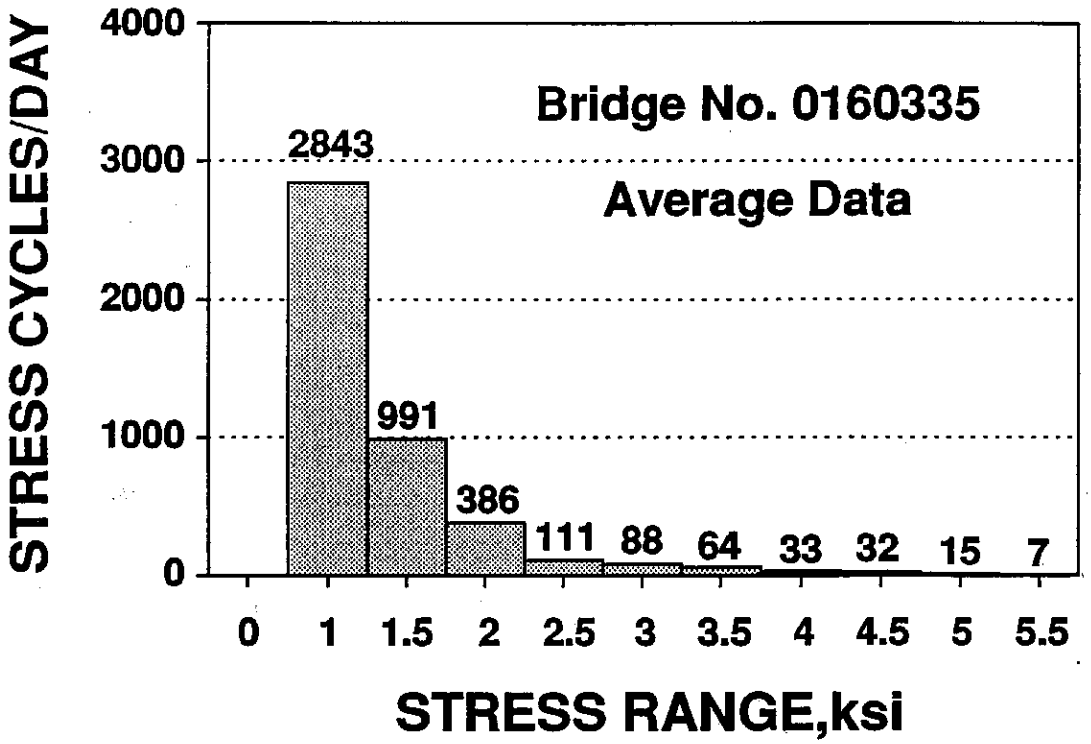

Figure 3. Stress range-frequency histogram for a major metropolitan feeder route, US 12 & 45 (Mannheim Road near O'Hare Airport), carrying a large traffic volume, and a full spectrum of light to heavy commercial vehicles.

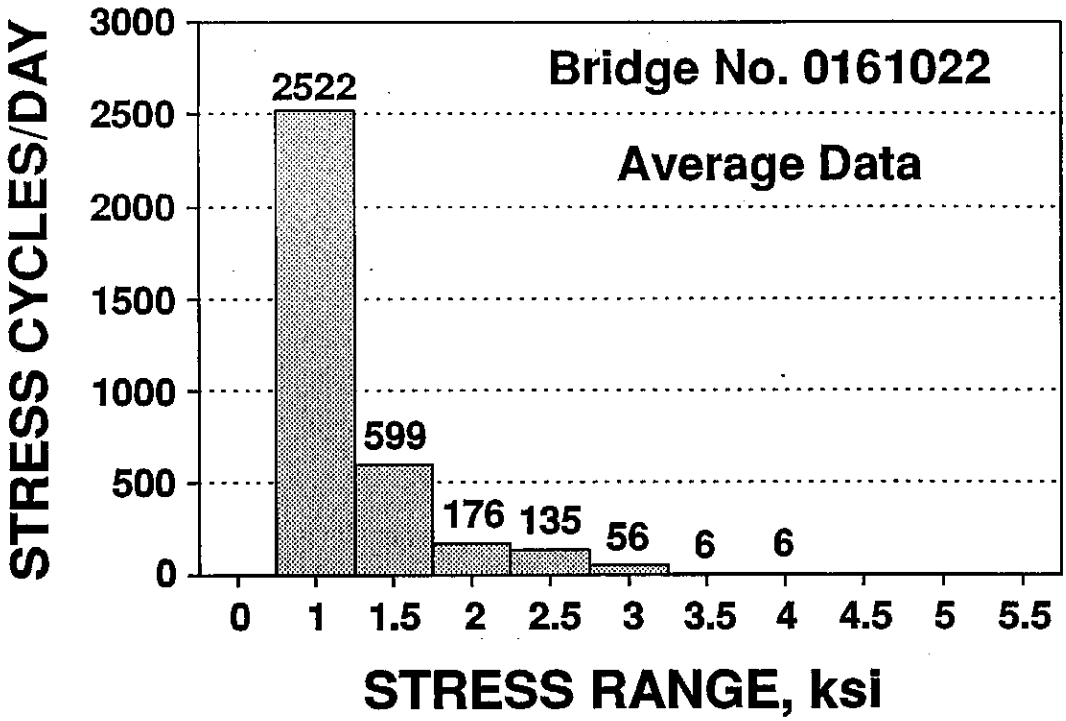

Figure 4. This bridge carries Illinois Route 83 traffic over the Cal Sag Channel Extension near Lemont. The main span is an overhead truss, the approach spans are simply supported, multiple stringer spans. The structure typically carries 28,000 ADT with 2,000 commercial ADT. Strain gages were installed at mid-span of one of the approach spans. The pertinent fatigue detail is a rolled section in bending.

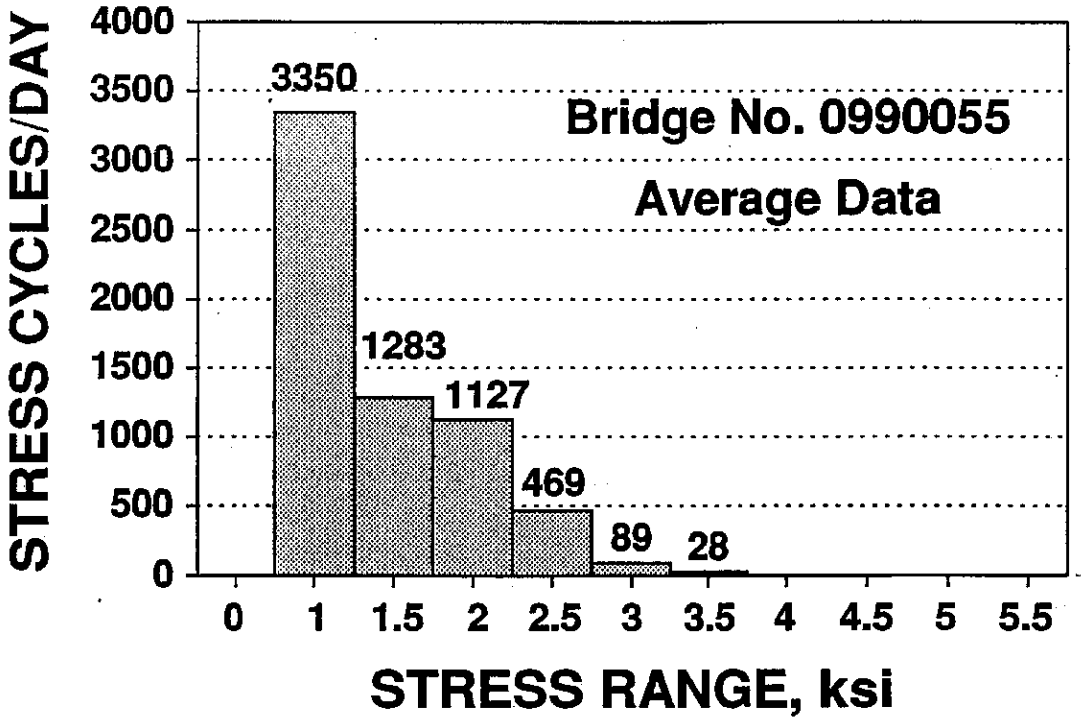

Figure 5. This bridge carries I-80 eastbound traffic over southbound Center Street in Joliet. The bridge is a simply supported, multiple stringer, single span structure. The bridge typically carries 21,000 ADT with 8,550 commercial ADT. Strain gages were installed near the flange thickness transition welds. Welds were ground smooth and radiused.

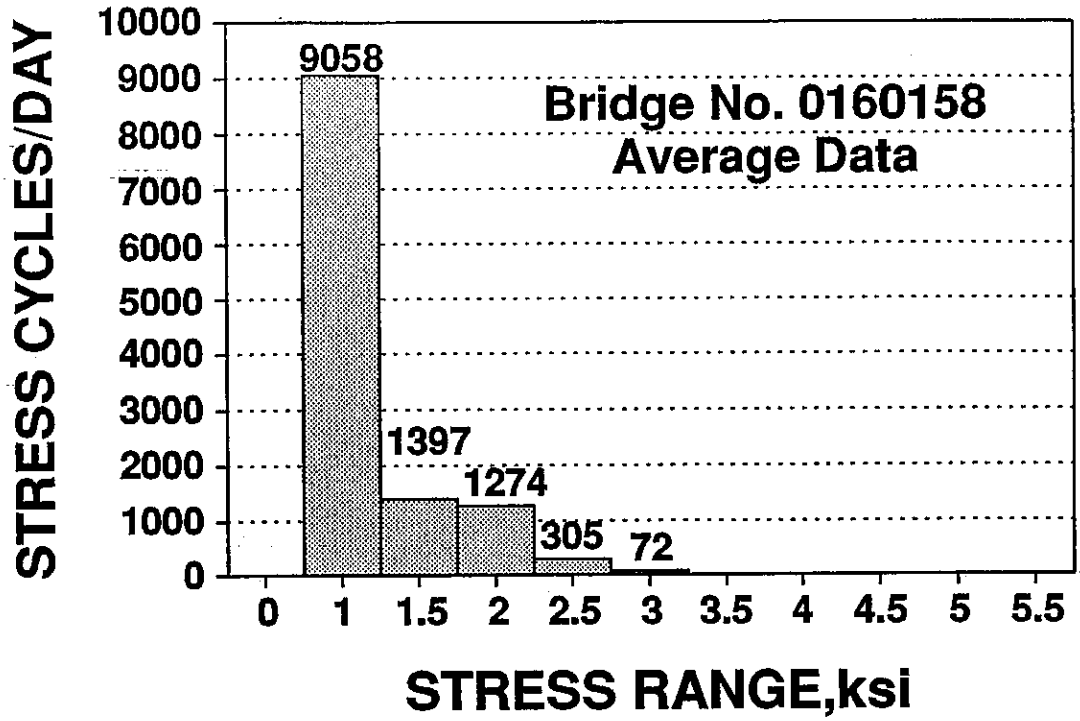

Figure 6. This bridge carries I-94 (Calumet Expressway) southbound traffic over the Little Calumet River in Chicago. The main span is an overhead truss and the approach spans are composed of simply supported, multiple stringer sections. The structure typically carries 51,200 ADT with 15,800 commerical ADT (Average Daily Traffic). Strain gages were installed on main vertical truss members due to problems with access to the underside of the bridge.

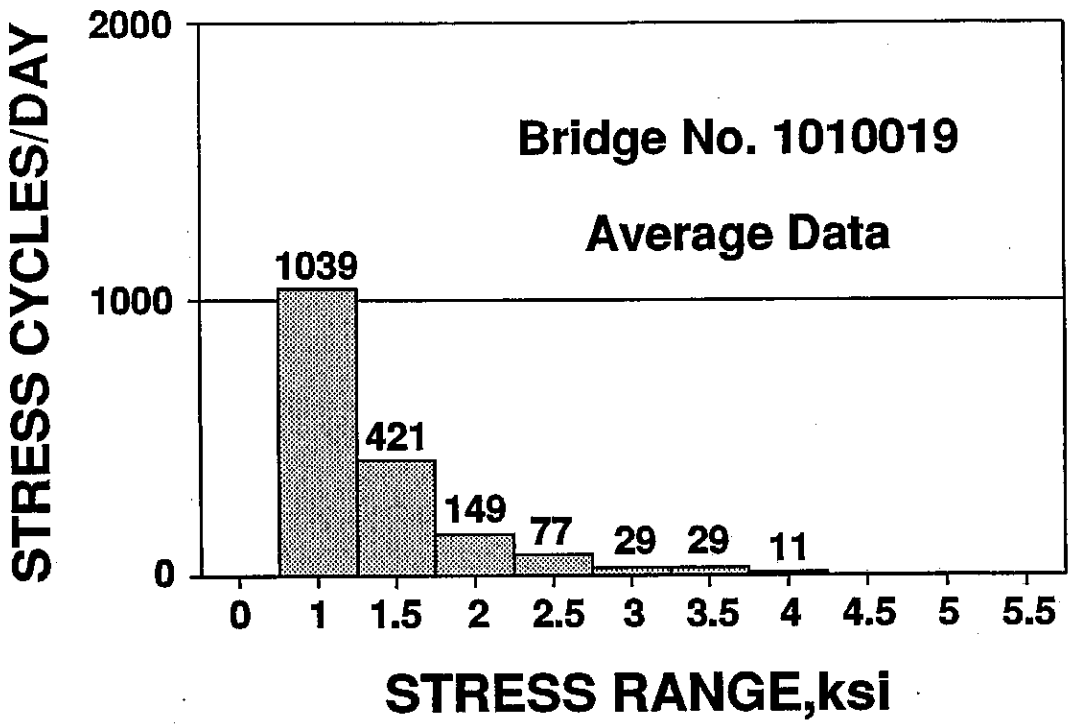

Figure 7. This bridge carries U.S. Route 20 westbound traffic over Grove Creek, approximately 15 miles west of Rockford. It is a three-span, continuous structure with multiple stringers and welded cover plates. The bridge typically carries 4,150 ADT with 900 commercial ADT. Strain gages were installed at the ends of the welded cover plates.

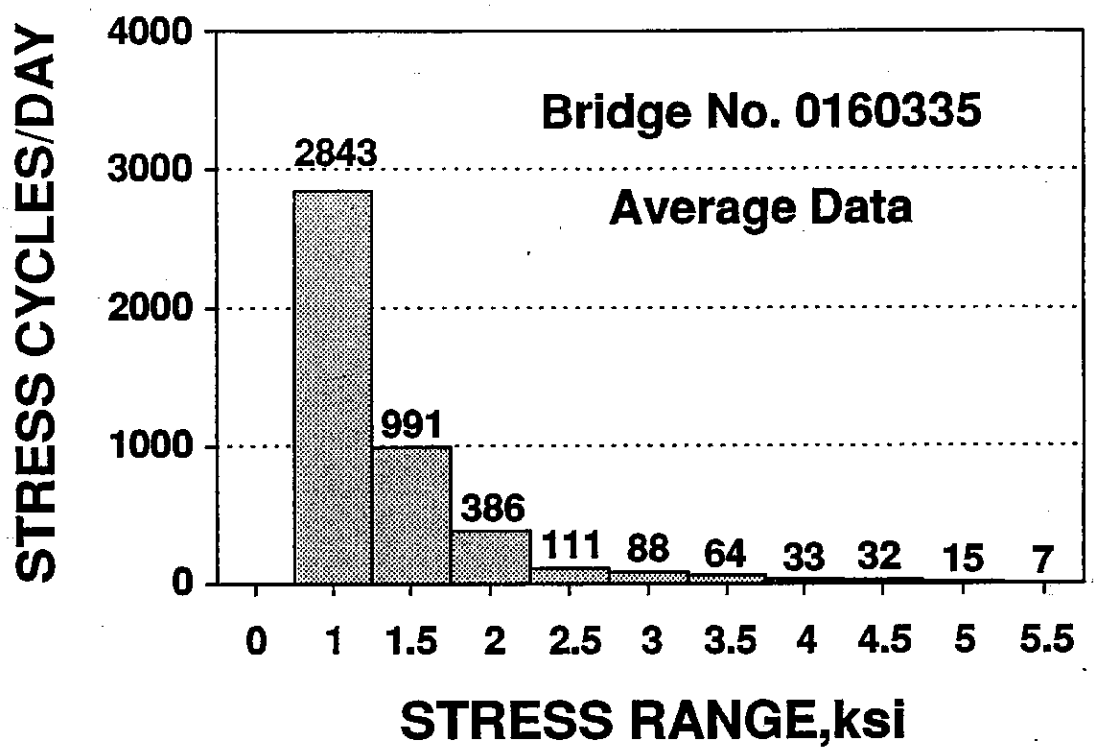

Figure 8. This bridge carries U.S. Routes 12 & 45 (Mannheim Road) traffic over Franklin Avenue and the Soo Line railroad yard in Franklin Park. The bridge is composed of several continuous sections. The structure typically carries 47,000 ADT with 4,350 commerical ADT. Strain gages were installed at the ends of welded cover plates.

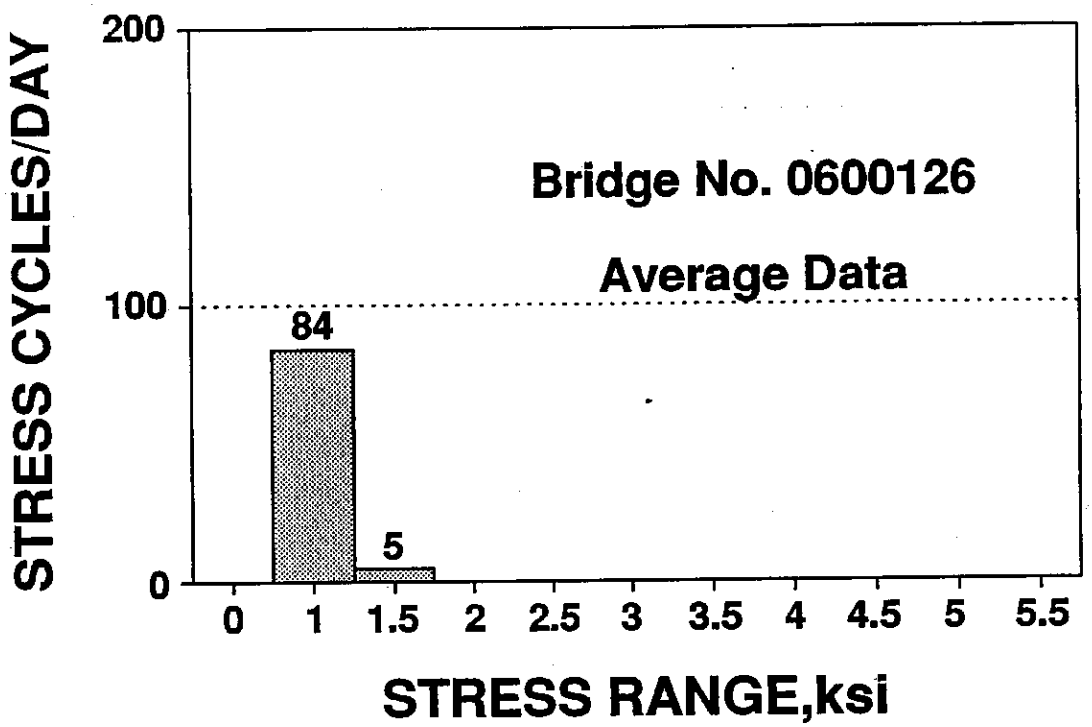

Figure 9. This bridge carries Illinois Route 111 northbound traffic over the Cahokia Canal near Fairmont City. It is a continous steel structure with riveted stringers and cover plates. It typically carries 3,400 ADT with 850 commercial ADT. Strain gages were installed at the ends of the riveted cover plates.

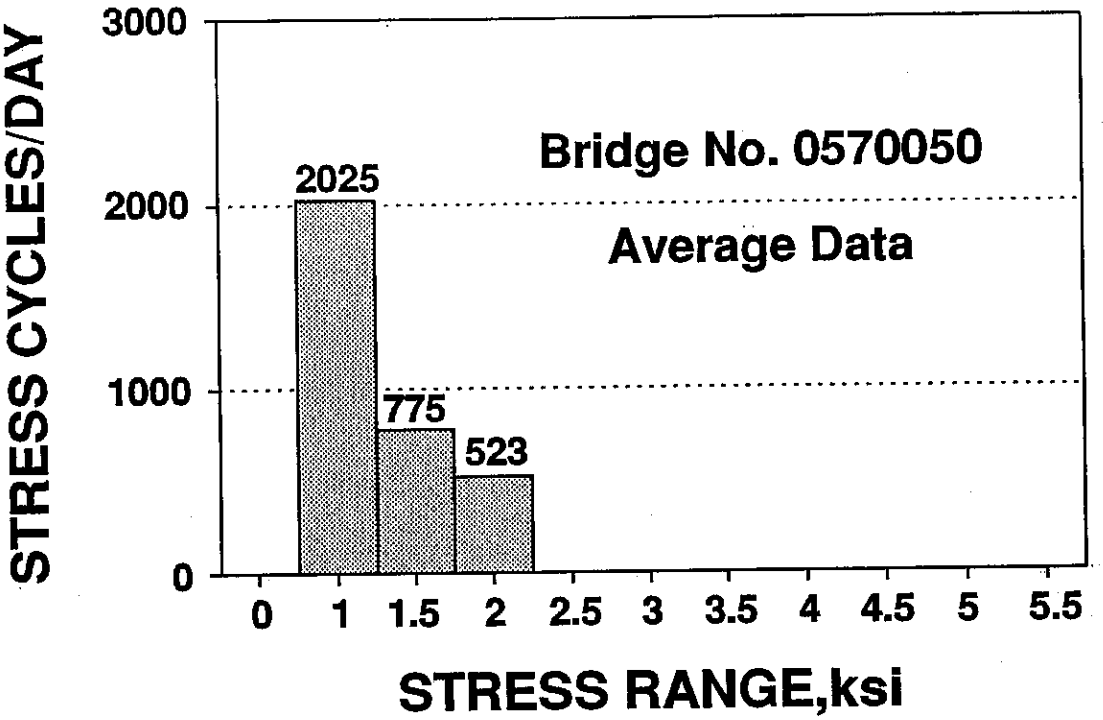

Figure 10. This bridge carries U.S. Route 51 traffic over the Mackinaw River approximately 12 miles north of Bloomington-Normal. This bridge is a three span, non-redundant, through-girder and floorbeam structure. It typically carries 8,009 ADT with 1,700 commerical ADT. Strain gages were installed at mid-span on each girder. Fatigue detail is a welded plate girder.

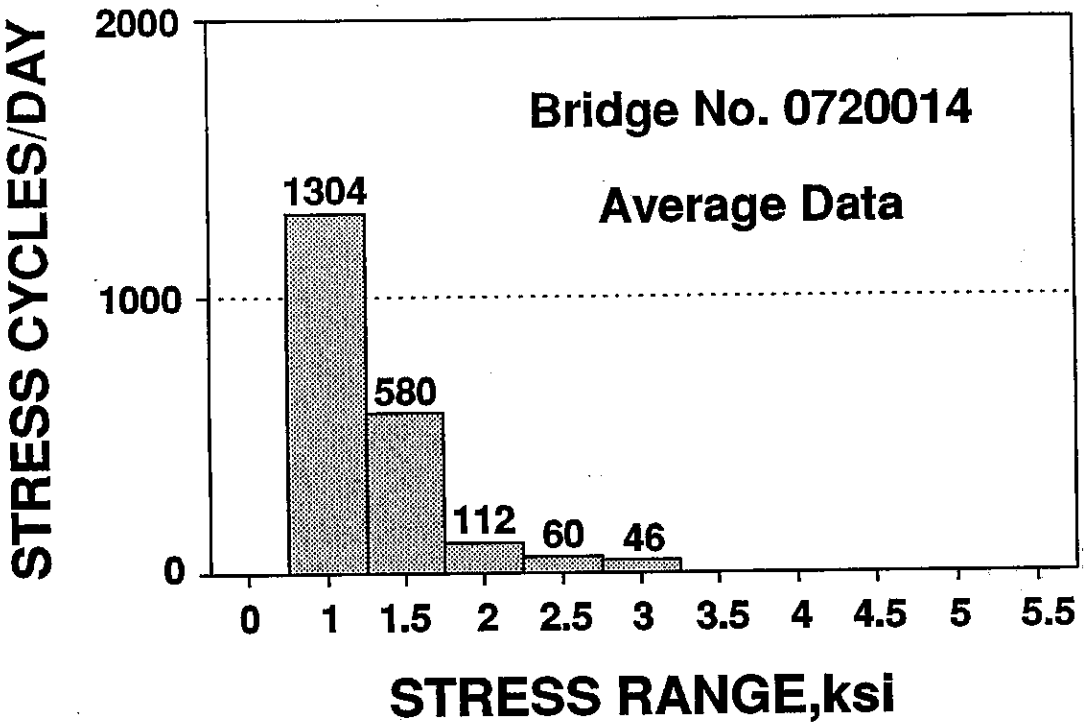

Figure 11. This bridge carries Illinois Route 29 traffic over Senechwine Creek north of Chillicothe. It is a three-span continuous steel structure with multiple stringers and welded cover plates. It typically carries 6,400 ADT with 500 commerical ADT. Strain gages were installed at the ends of the welded cover plates.

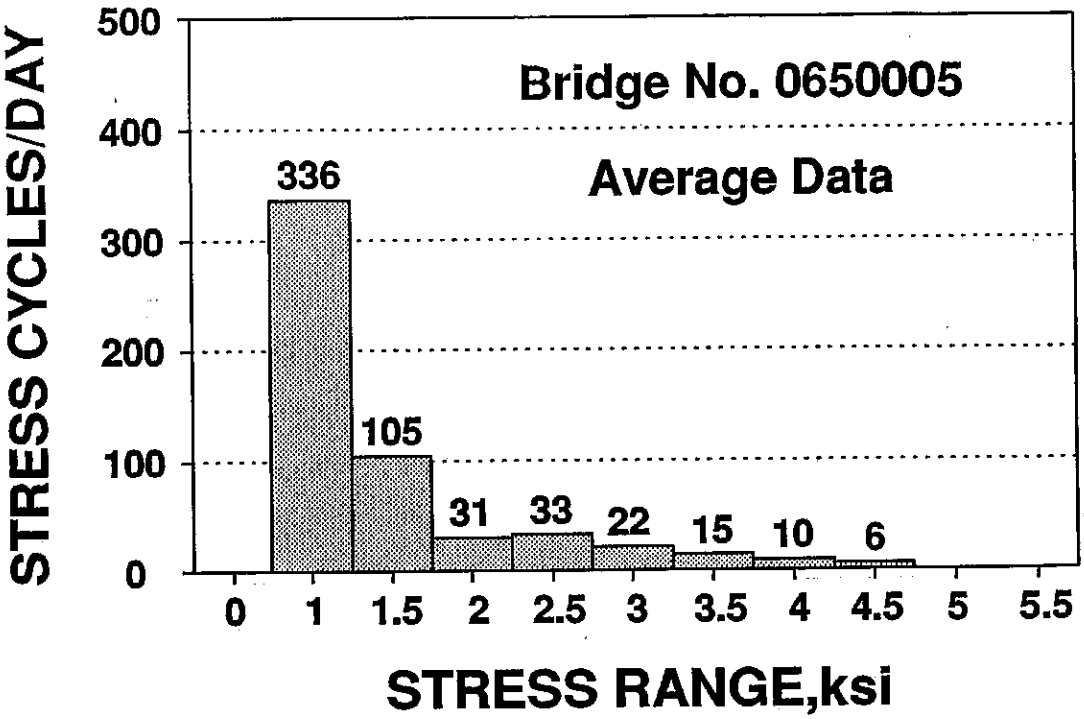

Figure 12. This bridge carries Illinois Route 97 traffic over the C & IM (Chicago and Illinois Midland) Railroad near Petersburg. It is a continuous steel structure with multiple stringers and welded cover plates. It typically carries 2,900 ADT with 200 commerical ADT. Strain gages were installed at the ends of the welded cover plates.

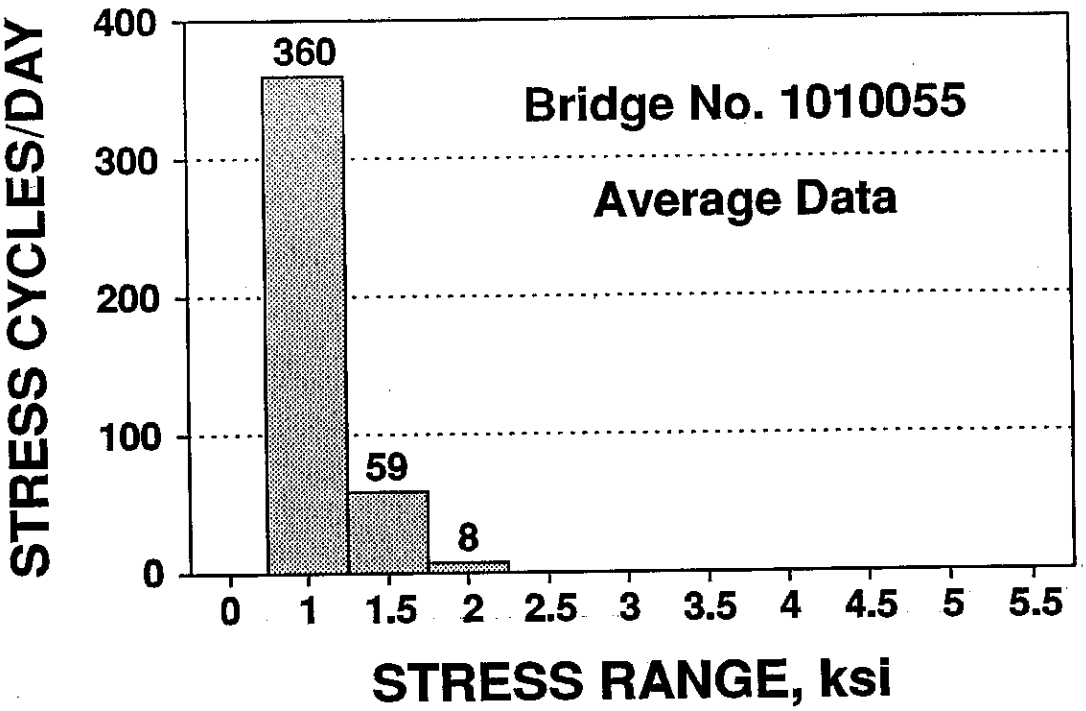

Figure 13. This bridge carries U.S. Route 20 eastbound traffic over Illinois Route 2 in Rockford. This structure has cantilevered side spans with pin and link connections for thermal expansion. The structure carries typically 6,400 ADT with 900 commerical ADT. Strain gages were installed at the maximum stress area in the link plates, near the pin. This fatigue detail is a tensioned plate with a large hole. Disparity of histogram to that of Figure 14 is largely due to construction activity.

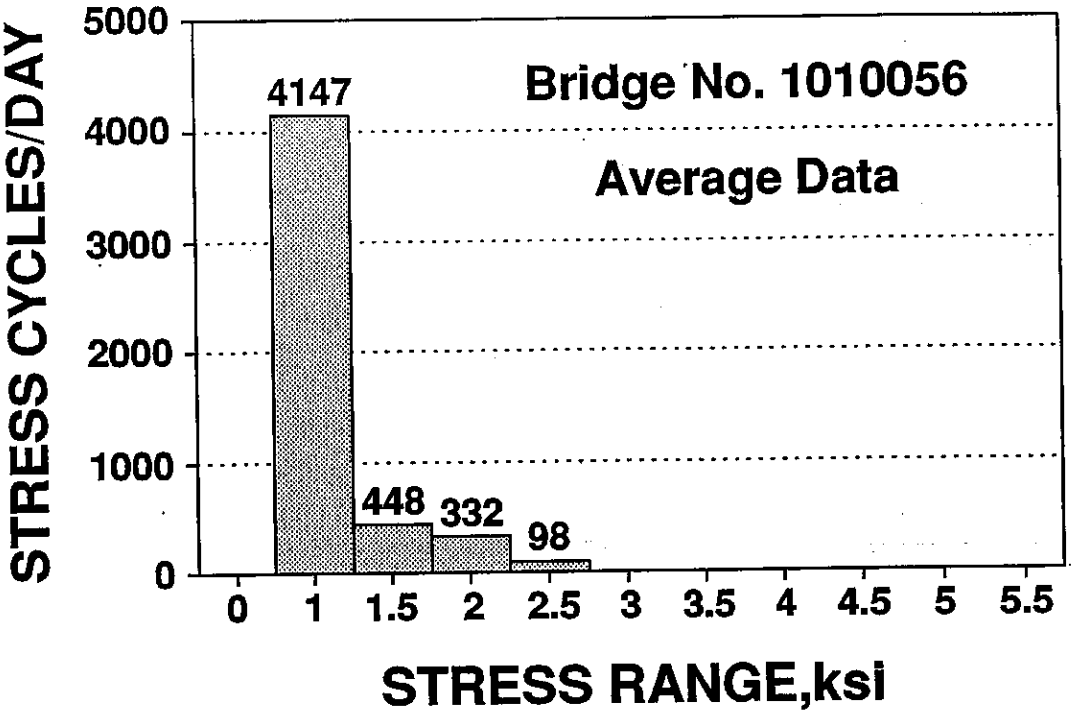

Figure 14. This bridge carries U.S. Route 20 westbound traffic over Illinois Route 2 in Rockford. This structure has cantilevered side spans with pin and link connections for thermal expansion. The structure typically carries 6,400 ADT with 900 commercial ADT. Strain gages were installed at the maximum stress area in the link plates, near the pin. This fatigue detail is a tensioned plate with a large hole.

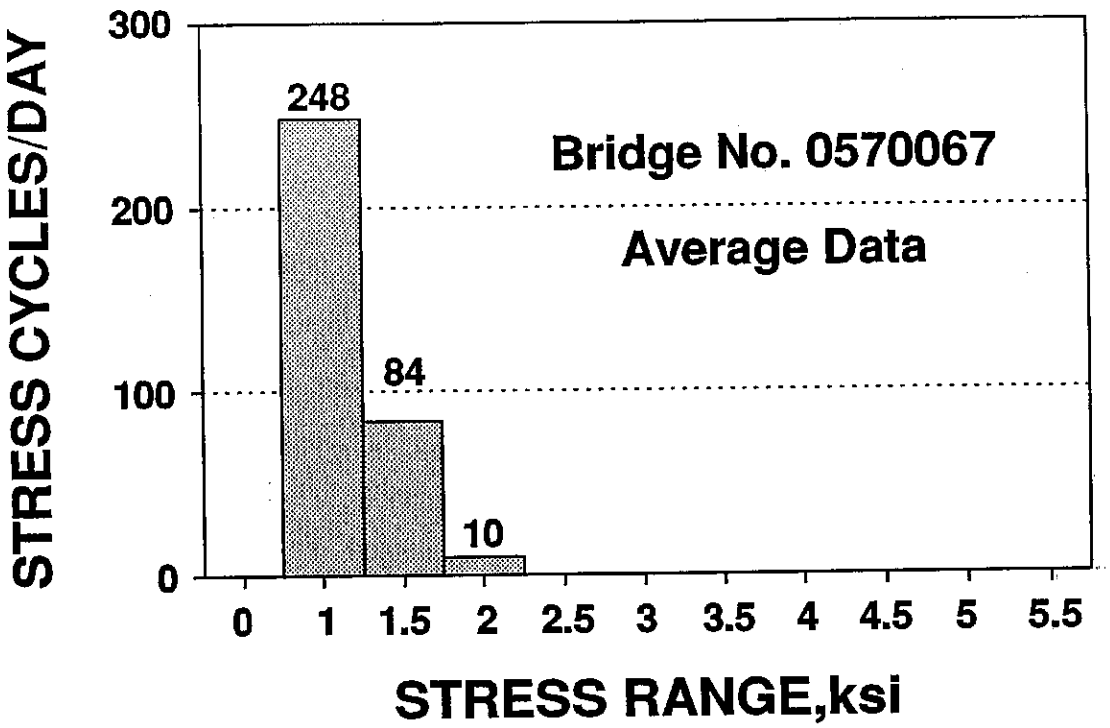

Figure 15. This bridge carries I-55 Business Loop southbound traffic over Sugar Creek in Bloomington-Normal. This structure is a simply supported, single span with multiple stringers. The structure typically carries 13,400 ADT with 850 commercial ADT. Strain gages were installed near mid-span. Fatigue detail is a smooth rolled section in bending.

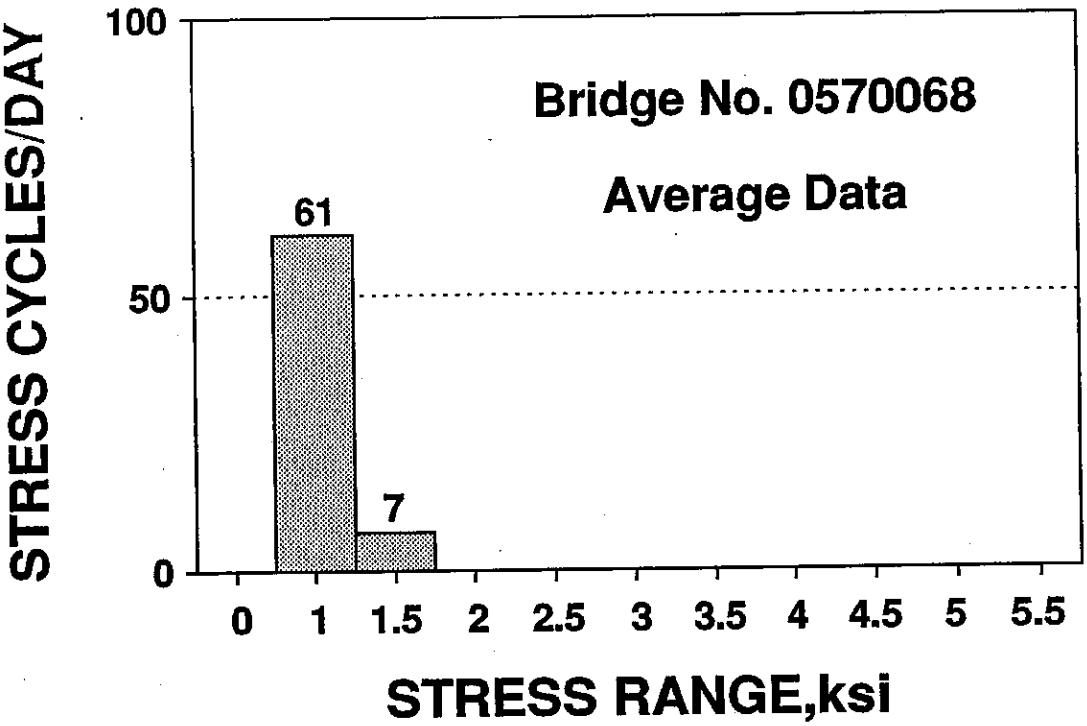

Figure 16. This bridge carries I-55 Business Loop northbound traffic over Sugar Creek in Bloomington-Normal. The structure is a simply supported, single span with multiple stringers. The structure typically carries 13,400 ADT with 850 commerical ADT. Strain gages were installed near mid-span. Fatigue detail is a smooth rolled section in bending.

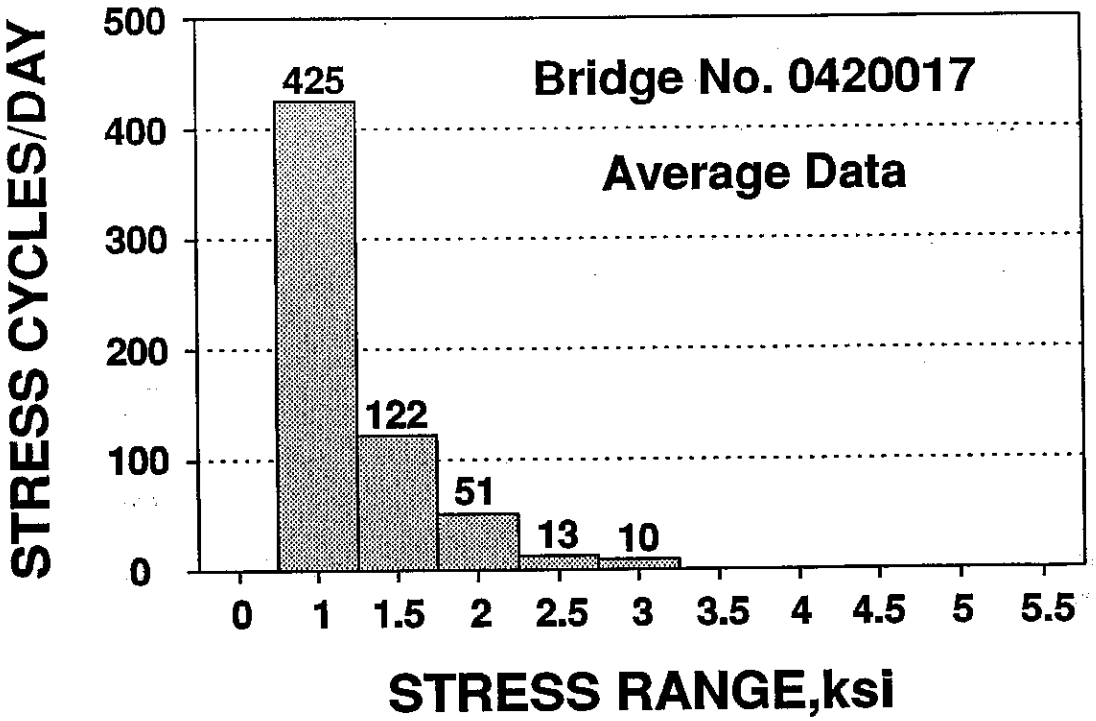

Figure 17. This bridge carries U.S. Route 67 traffic over Macoupin Creek near Rockbridge. It is a continuous steel structure with multiple stringers and welded cover plates. It typically carries 1,750 ADT with 375 commerical ADT. Strain gages were installed at the ends of the welded cover plates.

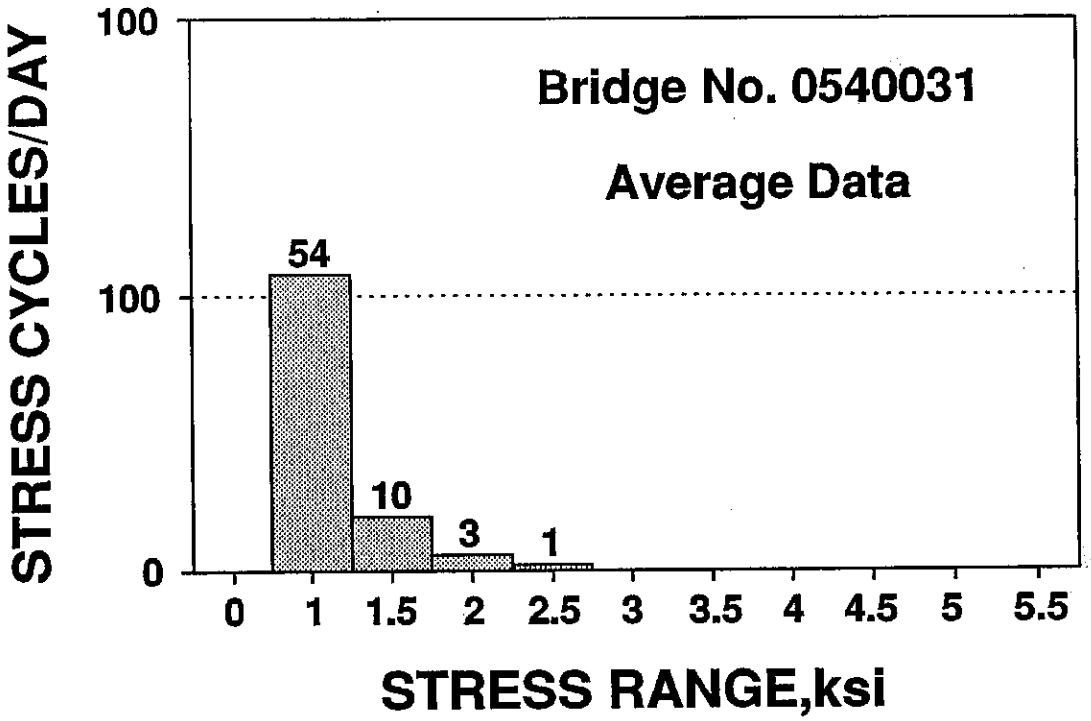

Figure 18. This bridge carries Illinois Route 54 traffic over Lake Fork Creek, approximately 12 miles northeast of Springfield. It is a continuous structure with multiple stringers and welded cover plates. It typically carries 1,150 ADT with 125 commercial ADT. Strain gages were installed at the ends of the welded cover plates.

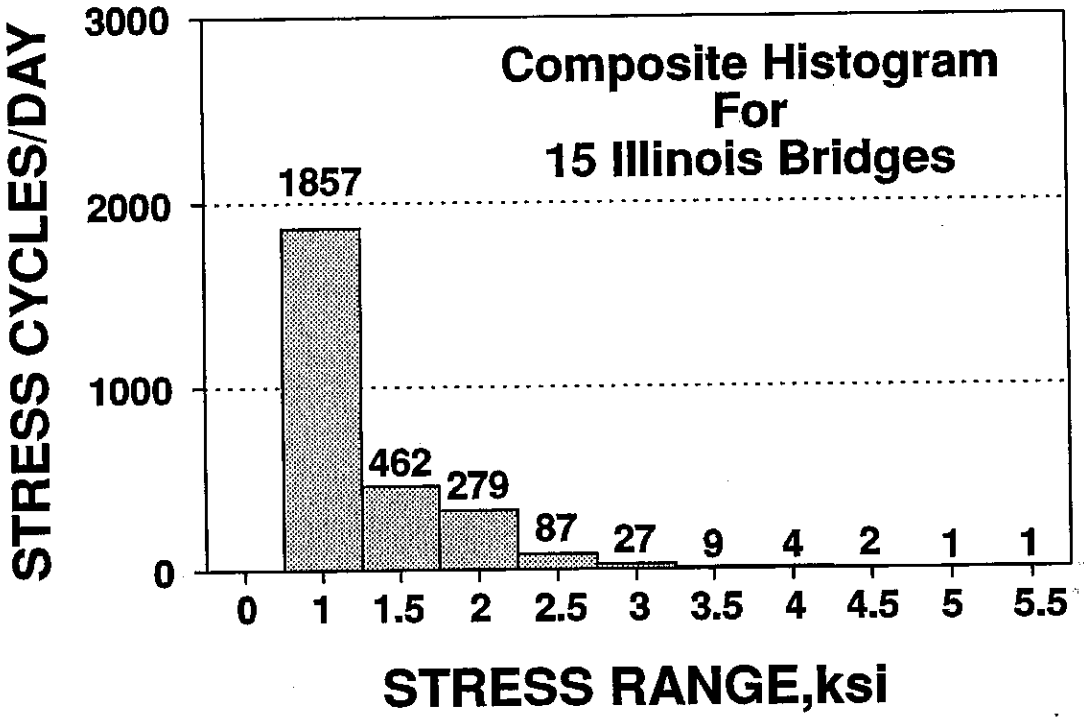

Figure 19. Composite stress range vs. frequency histogram for State of Illinois bridges, based on a mean of each stress range and frequency for 15 representative bridges. This data does not include bridges of movable, suspension, or tied-arch construction that span over major rivers like the Mississippi, Illinois or Ohio Rivers.

TABLE 4

SUMMARY OF STRESS RANGES AND FREQUENCIES
FOR 15 ILLINOIS BRIDGES STUDIED*

Bridge No.	Frequency, cycles/day at specific ksi stress range									
	1.0 ksi	1.5	2.0	2.5	3.0	3.5	4.0	4.5	5.0	5.5
0161022	2522	599	176	135	56	6	6	–	–	–
0990055	3350	1283	1127	469	89	28	–	–	–	–
0160158	9058	1397	1274	305	72	–	–	–	–	–
1010019	1039	421	149	77	29	29	11	–	–	–
0160335	2843	991	386	111	88	64	33	32	15	7
0600126	84	5	–	–	–	–	–	–	–	–
0570050	2025	775	523	–	–	–	–	–	–	–
0720014	1304	580	112	60	46	–	–	–	–	–
0650005	336	105	31	33	22	15	10	6	–	–
1010055*	360	59	8	–	–	–	–	–	–	–
1010056*	4147	488	332	98	–	–	–	–	–	–
0570067*	248	84	10	–	–	–	–	–	–	–
0570068*	61	7	–	–	–	–	–	–	–	–
0420017	425	122	51	13	10	–	–	–	–	–
0540031	54	10	3	1	–	–	–	–	–	–
mean	1857	462	279	87	27	9	4	2	1	1

* In cases where bidirectional interstate bridges are physically separated, traffic in both directions is reported. The stress cycles reported in this table are the mean outputs of all the gages placed on the bridge. The number of gages varies between 2 – 4 gages/bridge.

4. DETERMINATION OF FATIGUE DAMAGE

In order to determine the amount of damage suffered by certain fatigue-critical details on a bridge over a specified time period, a stress range-frequency histogram must be available for the ambient stresses affecting each of those details. Whether various welded details are fatigue critical or not must determined by a prior analysis of the bridge plans, calculations or other historical experiences of cracking with certain details.

Since the histogram is based on a 24-hour interval, it is simply multiplied by the number of days in the time period in question. Typically, this time period may be 25-50 years, depending on what the planning or design engineers determine to be a reasonable time period for bridge life extension or its functionality based on width, number of lanes, safety aspects or maintainability.

For each stress range in the histogram, the number of days in the time period multiplied by the frequency/day represents the number of damage cycles sustained by that detail. The amount of damage is then compared with known sustainable fatigue damage curves previously determined for many structural details on behalf of the AWS, AASHTO, DOD, SAE, and other organizations. The AWS Structural Welding Code for Steel provides conservative stress vs. number of cycles (S-N) plots for various details placed in categories. Data can also be plotted as N-S curves, where N is the dependent variable instead of stress range. In this report, the 50% mean data of Munse and co-workers[4] and the AWS Structural Welding Code/Steel[2] fatigue categories for various fatigue-prone details are used.

The Palmgren-Miner linear damage rule is then employed to quantify damage:

$$\sum_{i=1}^{n} \frac{n_{sri}}{N_{sri}} = \frac{n_{sr1}}{N_{sr1}} + \frac{n_{sr2}}{N_{sr2}} + \frac{n_{sr3}}{N_{sr3}} + .. = 1 \quad (2)$$

where: n_{sri} = number of stress cycles at a specific 0.5 ksi stress interval

N_{sri} = number of stress cycles sustainable at that stress level to cause severe cracking or failure

The linear damage rule, although an approximation, has been widely used in fatigue studies because of its directness and simplicity, and for its ease of handling of the statistical nature of fatigue. The tensile test of a metallic or non-metallic specimen constitutes one damage event n, that consumes 100% of its fatigue life N, or n/N = 1.00. Proportionally smaller fatigue events, such as 1,000 recurring truck overloads of a cover plate weld at 20 ksi stress range may result in cumulative damage of only 0.004, or 0.4% of its available fatigue life.

In the linear damage rule, n_1 is an individual number of fatigue damage events occurring at a particular stress, whereas N_{sr1} is the total number of permissible damage events at that stress level before significant cracking or rupture occurs.

Each specific N_{sr1}, N_{sr2}, N_{sr3} and so on can be calculated from published data for each specific stress range in the histogram by knowing the number of cycles to failure vs. stress range (N-S) equation for each detail affected. The equation takes the form:

$$N_f = c[S]^m \quad (3)$$

where: S = stress range, ksi

c = fatigue strength coefficient

m = fatigue strength exponent

N_f = number of cycles to major crack formation or failure.

This equation is a rearranged form of Basquin's equation for high cycle fatigue. High cycle fatigue is characterized by elastic and low plastic strain levels. Low plastic strains result from applied stresses that are near or slightly above the yield stress of the material. High cycle fatigue generally means that fatigue lives are in excess of 10^4 cycles. Tables 5a and 5b summarize typical high cycle fatigue exponents and coefficents for various details using the 50 percent mean data of Munse, et al., and the AWS Structural Welding Code fatigue categories for steel weldments, respectively.

In summary, the strain gages and load spectra instrumentation and time period determine the individual n_i values, whereas the respective available stress cycle capacities (N_i values) of sustainable fatigue damage for each stress range level are calculated by use of the above N-S equations for the detail in question.

The following sample calculation from the stress range-frequency histogram of Bridge 0160335 illustrates the method of fatigue damage assessment. The fraction of life consumed after 25 years of traffic exposure is calculated. First, the total life available at each 0.5 ksi stress level is calculated from the 50 percent mean fatigue detail N-S equation for a cover plate or from the AWS Structural Welding Code fatigue categories. Welded cover plates are classified as Category E. The

coefficient c and exponent m can be found in Table 5a (mean data) or Table 5b (AWS data). Then the total number of stress cycles sustained according to the stress-frequency diagram of Figure 20 is multiplied by 9125, which is the number of days in 25 years. Each n_i/N_i proportion is then added together to yield the total life consumed. The sample calculation uses 50 percent mean data, resulting in a fatigue life equation of

$$N = [4.218 \times 10^9]S^{-3.256} \qquad (4)$$

for a cover-plated beam, using the appropriate coefficient and exponent as found in Table 5a. Calculations are summarized in Table 6. The net result of this calculation is that 6.76% of the fatigue life of the cover plate has been consumed after 25 years. The amount of damage D incurred in one year is equal to 0.0027. The expected life span L, sustaining the same rate of damage each year is L = 1/D, or 1/0.0027 = 370 years.

It is emphasized that the 0.5 ksi increments used in this particular calculation are not fixed for the method in general but were related to the calibration of the DataMyte instrumentation. Different stress range increments may be obtained by changing the calibration of the strain gage data acquisition system in use, since the method is integrating the area under the stress range - frequency histogram.

TABLE 5a

Fatigue Strength Coefficients and
Exponents for Typical Structural Details,
50 % Mean Data*

Detail Description	Fatigue Coefficient, c	Fatigue Exponent, m
Wide flange with cover plate in bending	4.218×10^{9}	-3.256
Flange change in thickness with radiused ground weld joint (no width change)	1.318×10^{14}	-5.662
Slot or plug welds in tension	2.492×10^{9}	-3.146
Attachments to flanges, not radiused or ground	2.744×10^{9}	-3.195
Ordinary wide flange in bending (no attachments)	2.935×10^{16}	-6.622
Flat bars in tension attached to larger plate with side fillet welds	1.964×10^{10}	-4.050
Sharp changes in flange width, no radius	4.842×10^{9}	-3.517

*Based on the 50% mean data of Munse, et al[4]; stress in ksi. To obtain MPa, multiply by 6.89.

TABLE 5b

Fatigue Strength Coefficients and
Exponents for Typical AWS Structural Welding Code
Fatigue Stress Categories for Redundant & Non-Redundant Structures

Redundant Structures

Fatigue Category	Fatigue Coefficient, c	Fatigue Exponent, m
A	5.704×10^{10}	-3.240
B	1.848×10^{10}	-3.169
C	1.442×10^{10}	-3.459
D	1.720×10^{9}	-2.965
E	1.274×10^{9}	-3.105

Non-Redundant Structures

A	1.862×10^{12}	-4.754
B	4.221×10^{10}	-3.930
C	2.225×10^{11}	-5.032
D	3.536×10^{8}	-2.911
E	2.406×10^{8}	-3.077

TABLE 6

Damage Calculation Summary for Bridge 0160335, Cover-Plated Beams With 25-Year Traffic Exposure

Stress, ksi	Total Cycles Available, N_i*	Stress Cycles/Day	Stress Cycles Sustained After 25 Yrs, n_i	Incremental Fraction of Life Consumed, n_i/N_i
1.0	4.22×10^9	2843	2.59×10^7	.0061
1.5	1.13×10^9	991	9.04×10^6	.0080
2.0	4.42×10^8	386	3.52×10^6	.0080
2.5	2.14×10^8	111	1.01×10^6	.0047
3.0	1.18×10^8	88	8.03×10^5	.0068
3.5	7.14×10^7	64	5.84×10^5	.0082
4.0	4.62×10^7	33	3.01×10^5	.0065
4.5	3.15×10^7	32	2.92×10^5	.0093
5.0	2.23×10^7	15	1.37×10^5	.0061
5.5	1.64×10^7	7	6.39×10^4	.0039
Total fraction of life consumed in cover plate after 25 years of traffic per histogram				0.0676

*Using $N = [4.218 \times 10^9]S^{-3.256}$ as the fatigue life equation for cover plates.

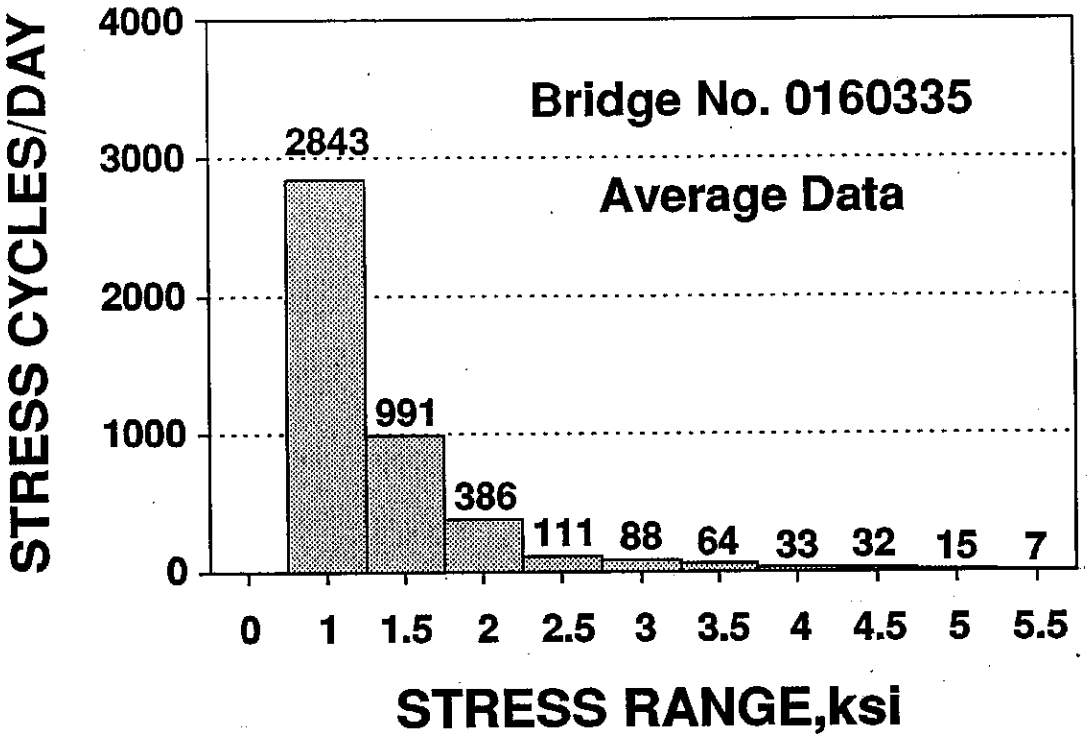

STRESS (KSI)	STRESS CYCLES PER DAY
1.0	2,843 x 9125* = n_1
1.5	991 x 9125 = n_2
2.0	386 x 9125 = n_3
2.5	111 x 9125 = n_4
3.0	88 x 9125 = n_5
3.5	64 x 9125 = n_6
4.0	33 x 9125 = n_7
4.5	32 x 9125 = n_8
5.0	15 x 9125 = n_9
5.5	7 x 9125 = n_{10}

*No. of days in 25 yrs.

Figure 20. Stress Range vs. Frequency/Day Multiplied by the Number of Days in 25 years.

5. EFFECT OF INCREASE FROM 72-KIP TO 80-KIP GROSS VEHICLE WEIGHTS

The purpose of this comparison was to obtain a reasonable estimate of the difference in measured maximum stress range between a truck weighing 72,000 lbs. and the same truck weighing 80,000 lbs. This allowable maximum weight increase went into effect in Illinois in 1983. The truck used for this experiment was a 3S-2 configuration (5-axle semitractor-trailer combination). The material used to load the truck was coarse aggregate. The bridge selected for the experiment was Illinois Route 54 over Lake Fork Creek in Logan County (Structure No. 0540031). This bridge was selected because it had convenient access, had strain gages already installed, and has low traffic volume. The instrumentation used to collect the data included weldable, electrical resistance foil strain gages, signal conditioners, and a chart recorder to record the analog signal. The two instrumented sections were each approximately three feet from the centerline of the roadway as shown in Figure 21. The test sequence consisted of the truck passing over the bridge at highway speed (55 mph) in both directions, taking care to make sure no other vehicles were on the bridge. Several test cycles were run for both loads. The actual weight of the truck was 81,700 lbs. for the 80-kip test and 72,350 lbs. for the 72-kip test. Figure 22 shows the typical response due to the 80-kip truck in either direction. The fluctuational nature of the loading is seen even though careful efforts were made to insure uniform crossing of the bridge each time. Figure 23 shows the typical response to the 72-kip truck. Table 7 lists the minimum and maximum live load stress ranges measured in the experiment, plus the overall mean stress ranges for all gages at each truck weight.

Based on the limited scope of the experiment, comparison of the combined mean stress ranges for the nominal 80 kip (82 actual) and 72 kip truck weights indicates an increase of 14.1% in the maximum stress range in the main load carrying members. A 14.1% increase derived from actual strain gage readings approximates the assumption that stress range increases linearly with applied load for common multi-girder bridges. The actual increase in truck weight from 72 kips to 82 kips is 12.9 percent (excluding impact effects). Much of the variation in strain gage readings comes from load sharing and the inability of the truck to maintain perfect retracing of each traverse of the bridge at high speeds.

TABLE 7

MAXIMUM STRESS RANGES MEASURED FOR 72 VERSUS 80 KIP NOMINAL VEHICLE WEIGHT COMPARISON

TEST NO.	GAGE NO.	ACTUAL TRUCK WEIGHT, (kips)	DIRECTION OF TRAVEL	STRESS RANGE, (ksi)
1	1	81.7	WB	3.18
1	2	81.7	WB	1.54
2	1	81.7	EB	2.74
2	2	81.7	EB	2.20
3	1	81.7	WB	2.96
3	2	81.7	WB	1.54
4	1	81.7	EB	2.52
4	2	81.7	EB	2.09
5	1	72.4	WB	2.85
5	2	72.4	WB	1.32
6	1	72.4	EB	2.09
6	2	72.4	EB	1.90
7	1	72.4	WB	2.99
7	2	72.4	WB	1.21
mean, 72 nom. 1, 2		72.4	EB&WB	2.06 ± .75
mean, 80 nom. 1, 2		81.7 (12.8% increase)	EB&WB	2.35 ± .61 (14.1% increase)

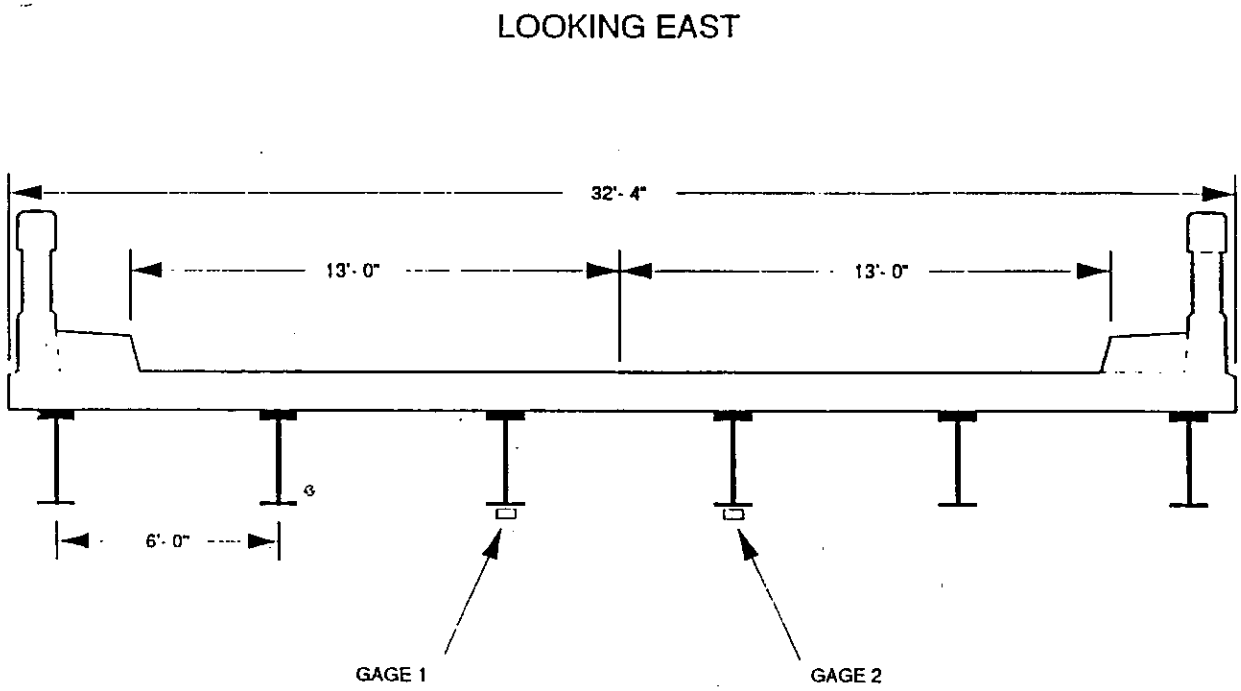

Figure 21. Cross-section of instrumented area of Illinois Route 54 over Lake Fork Creek. (Not to scale).

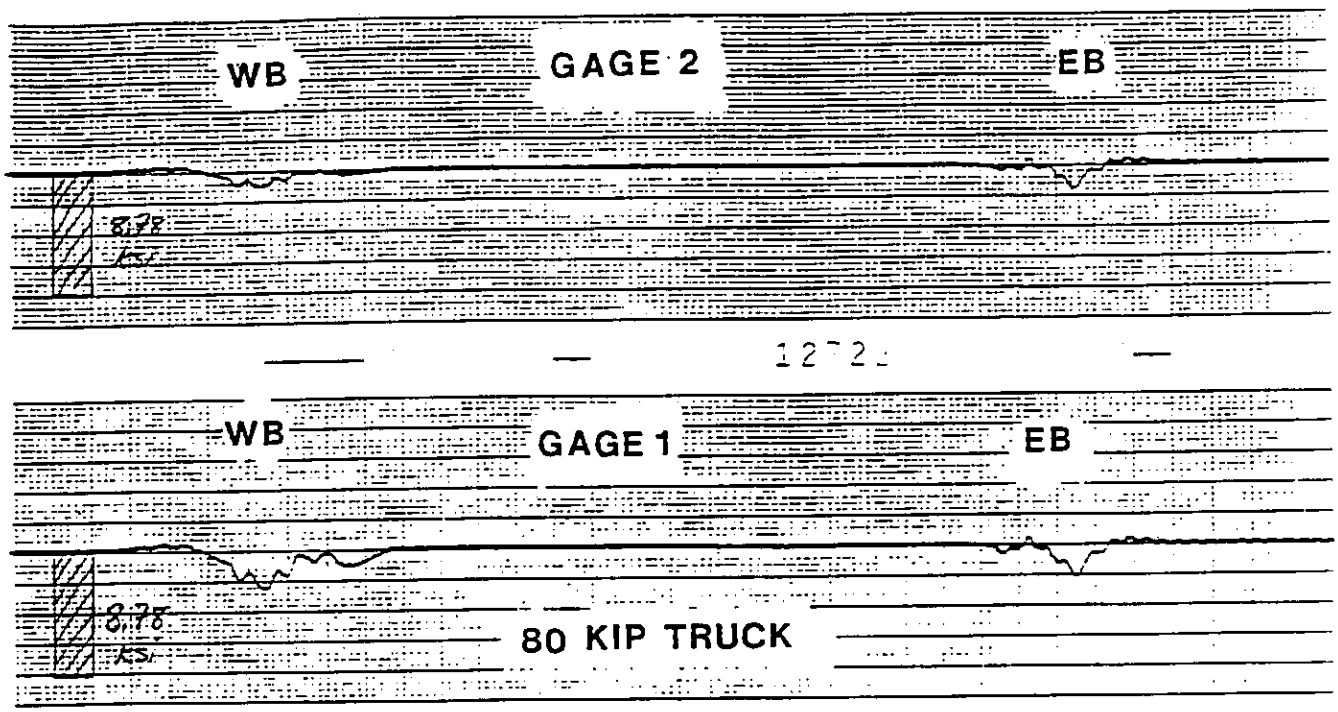

Figure 22. Typical response of strain gages to 80-kip nominal (82-kip actual) truck.

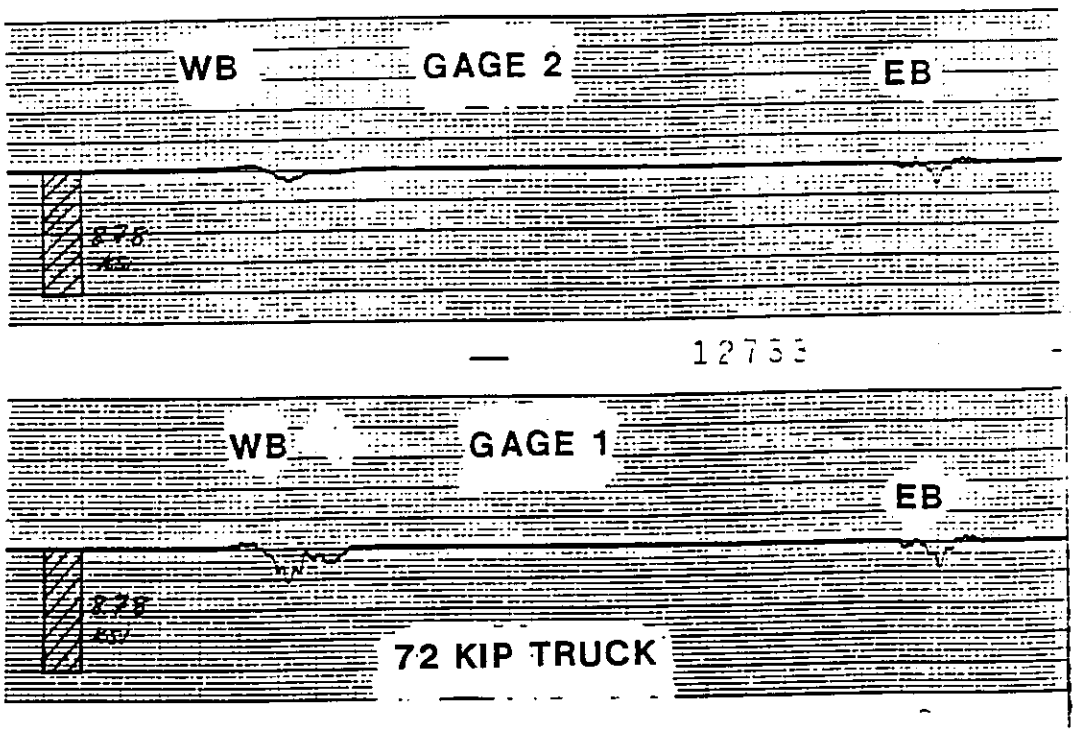

Figure 23. Typical response of strain gages to 72-kip truck.

10 percent increase in weight limits and a 5 percent traffic growth after 25 years, as shown in Table 8. The 10 percent weight increase is an approximation of the maximum truck weight increase from 73,280 pounds to 80,000 pounds which occurred in 1983 in Illinois. The 5 percent traffic increase is a statewide average of growth patterns in Illinois over the 1983-1988 time period. Increased truck weight and traffic causes 4.5 times as much fatigue damage compared to no growth of traffic and weight. It is interesting to note that a 5 percent growth rate compounded annually for 25 years results in an increase of 3.386 times the original number of applied stress cycles. Thus, the annual progressive increase of traffic alone will significantly increase fatigue damage to a bridge.

TABLE 8

Damage Calculation Summary for Bridge 0160335, Cover-Plated Beams With 25-Year Traffic Exposure With 10% Truck Weight Increase and 5% Traffic Growth

New Stress Range, ksi*	Total Cycles Available, N_i	Stress Cycles Sustained After 25 Yrs. @ 5% Growth***	Incremental Fraction of Life Consumed
1.00**	4.22×10^9	8.97×10^7	.0208
1.65	8.26×10^8	3.06×10^7	.0370
2.20	3.24×10^8	1.19×10^7	.0367
2.75	1.57×10^8	3.42×10^6	.0218
3.30	8.65×10^7	2.72×10^6	.0314
3.85	5.23×10^7	1.98×10^6	.0379
4.40	3.39×10^7	1.02×10^6	.0301
4.95	2.31×10^7	9.89×10^5	.0428
5.50	1.64×10^7	4.64×10^5	.0283
6.05	1.20×10^7	2.16×10^5	.0180
Total Fraction of Life Consumed in Cover Plates After 25 Years Per Modified Histogram			.3048

*Assumes a 10 percent increase in heavy traffic weight, including light trucks and buses.

**Passenger car weight assumed to remain constant.

***A 5 percent growth rate compounded annually for 25 years results in an increase of 3.386 times the original value.

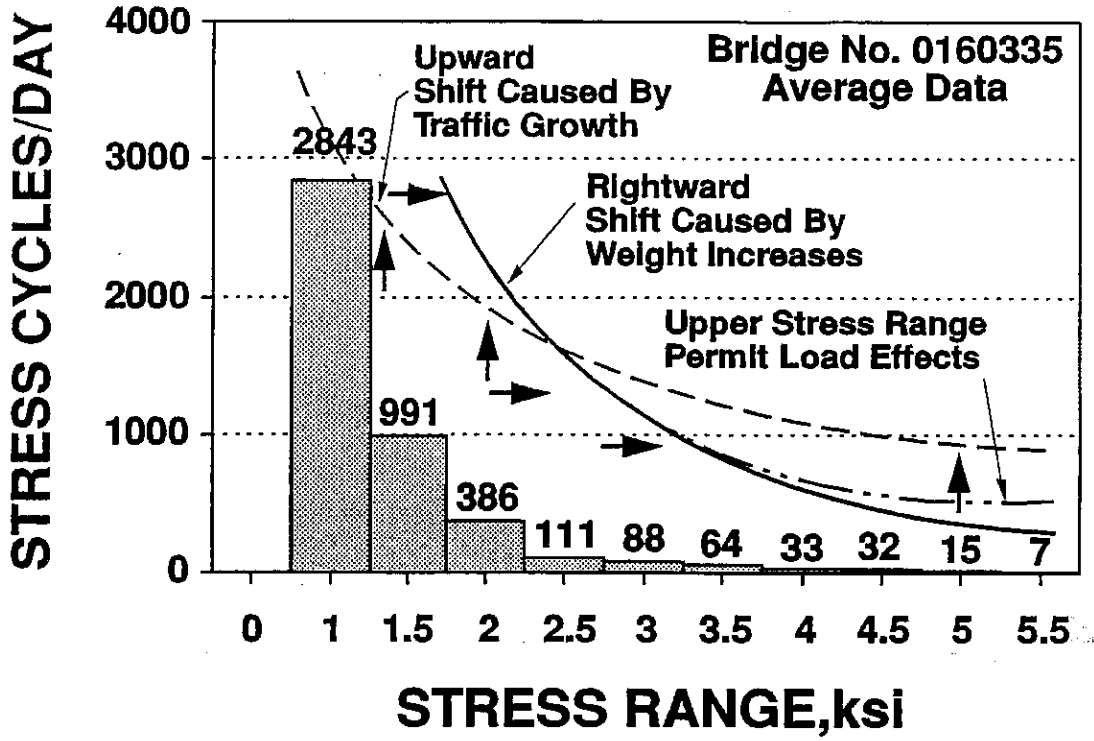

Figure 24. Schematic effects of permits, traffic, and truck weight growth on the stress range-frequency histogram.

7. CALCULATION OF SAFETY FACTOR FOR WELDED STRUCTURES

Welds constitute only part of an overall structure. The highest residual tensile stress fields in welds are largely confined to areas starting near the weld toes, increasing and then peaking at the weld bead centerline. Other localized portions of the structure may also be in compression induced by the residual tensile stress fields of the cooling welds[5] or are dead load compression zones of the structure itself. Although residual stresses are typically one of the principal contributors to crack initiation in welds, their effects are often dissipated by localized plastic deformation during cyclic loading. The crack may also be blunted by the compressive stress fields that may exist in the structure or by the inherent fracture toughness of the structural element itself. Improved fracture toughness is typically found in structural steels with fine grain sizes, lower carbon, sulfur and phosphorus contents, higher nickel and manganese contents, and other alloying additions which control inclusions and their distribution.

Residual stresses, coupled with discontinuities already present in the weld joint itself, lead to degradation of weldment fatigue life. Such discontinuities include lack of fusion, slag inclusions, porosity, lack of penetration, centerline cracks, and weld bead undercut, all of which significantly degrade the fatigue life of a weldment.[6, 7, 8]

Many structural welds contain such discontinuities, and therefore experimental tests of the fatigue lives of the same detail show marked scatter. Although weld joint geometry is not the sole determinant of weld fatigue strength, it can concentrate ambient gross-section stresses present in the structure.

Although the weld toe, its centerline, or the heat-affected zone (HAZ) may crack, this same weldment crack must propagate through considerable distances into base metals which are substantially more homogeneous than welds in order for catastrophic failure of the bridge to occur. These wrought materials remote from welds have virtually the same crack propagation characteristics of structural steels that were never welded. Since welds are only part of a structure, higher mean stresses sustained throughout the rest of the structure do have influence on overall structural safety. The presence of cracks in selective welds does not necessarily constitute a failure of the structure. However, as the mean stresses in the structure increase, the permissible critical crack lengths originating from those welds decrease.

One of the effects of higher mean tensile stress on fatigue crack growth rates in various steels is to establish a lower threshold ΔK for cracking compared to cyclic fatigue with lower mean stresses.[9, 10] Similar experimental results in both aluminum alloys and various steels show that a tensile mean stress decreases the permissible axial cyclic stress amplitude when compared to compressive values.[11]

The significance of mean stress effects has also been demonstrated in fatigue studies of butt welds of ASTM A 36 and ASTM A 514 by Lawrence.[12] This work shows that as mean stress becomes increasingly tensile and perpendicular to the weld axis, the high cycle fatigue strength decreases. This effect is particularly prominent in mild steel welds that have been shot-peened compared to those in the as-welded state.[13] Even lower strength welded structural steels such as ASTM A 36 in higher cycle fatigue regimes

are affected by increased mean stress ratio. Higher R-ratios (min. stress/max. stress) showed an approximately 10-15% reduction in butt weld fatigue life when R=1/2 was compared to R=0 at 2,000,000 cycles.[14] The studies cited above where increased mean stress decreased fatigue life pertained to welds that were stressed in the transverse direction. However, welds that are longitudinally stressed parallel to the weld axis apparently are insensitive to mean stress effects.[15] Nevertheless, since weld stresses are never perfectly aligned in any welded structure, mean stresses, in general, should be taken into account for safety purposes.

The safety factor in engineering fatigue and machine design is typically determined by use of either the Goodman, Soderberg, or Gerber fatigue failure equations. Although the conservative Goodman relationship is the most widely used, the Gerber parabolic equation most accurately represents actual experimental fatigue data:

$$N_{safety} = \frac{1}{(S_a/S_e) + (S_m/T_u)^2} \qquad (5)$$

Where: N_{safety} = safety factor

S_a = alternating stress amplitude, $(S_{max} - S_{min})/2$, ksi

S_m = mean stress, $(S_{max} + S_{min})/2$, ksi

S_{max} = maximum stress, ksi

S_{min} = minimum stress, ksi

S_e = fatigue strength at 2×10^6 cycles or 10^7 cycles, whichever is typical of actual or intended life span, ksi

T_u = minimum specified ultimate tensile strength of the steel, ksi.

However, bridge design literature and codes use a fatigue strength category for various details and stress ranges instead of

alternating stress amplitudes. Mean stress is a combination of both live load and dead load stresses. Therefore, a modification of the Gerber parabolic equation adapted to bridges is proposed which incorporates the actual fatigue strength of specific details and the stress range:

$$N_{safety} = \frac{1}{\frac{S_{LL}}{F_d} + \left[\frac{(S_{LL} + 2S_{DL})/2}{T_u}\right]^2} \qquad (6)$$

Where: N_{safety} = safety factor

S_{LL} = live load stress range, ksi

S_{DL} = dead load stress in member, ksi.

F_d = fatigue strength of detail at 2×10^6 or 10^7 cycles, depending on desired design life and average daily truck traffic

T_u = minimum tensile strength of the steel specified, ksi

In this new equation, live load stress range replaces alternating stress amplitude S_a in the Gerber equation, and the detail fatigue strength F_d replaces fatigue strength S_e. Mean stress S_m becomes [(live load stress range + dead load) + (dead load)]/2, which is the mean of dead load and live load stresses. This safety factor equation places primary emphasis on the proportion of the live load stress range to that of its detail fatigue strength. The remaining squared mean stress term is principally concerned with ambient dead load stress in the remainder of the structure. This term is a measure of the remaining elastic-plastic strain capacity, and becomes significant when ambient stresses start to approach bridge code allowable stresses. This term is also significant when steels with lesser notch plasticity such as ASTM A 514, A 588, or A 572 are used, or for lower strength steels like ASTM A 36 when used at lower temperatures.

Using the previous example of Bridge 0160335, a safety factor for the cover plates is calculated. The peak live load stress range (S_{LL}) developed in Bridge 0160335 was 5.5 ksi. The fatigue strength for cover plates at 2 x 10^6 cycles for 50 percent mean data is 10.5 ksi (F_d). This fatigue strength was chosen because the total number of cycles above 2.5 ksi in a 25-year design is 2,180,875 cycles. Assuming that the cover plate is near the point of counterflexure, its dead load stresses are fairly low. An estimated value of 4 ksi for dead load stress (S_{DL}) is used. A conservative value of 58.0 ksi is used for the tensile strength (T_u) of an ASTM A 36 rolled beam and weldment. Values of 65.0 ksi may be used for ASTM A 572 and 70.0 ksi for ASTM A 588. The calculated safety factor of the detail is therefore:

$$N_{safety} = \frac{1}{\frac{5.5}{10.5} + \left[\frac{(5.5 + 2 \times 4)/2}{58}\right]^2} = 1.86$$

For longer design lives of 50 years or more, the fatigue strength of the detail at 10^7 cycles should be used. If the fatigue strength at 10^7 cycles is used (6.5 ksi), the safety factor drops to 1.16, a warning sign. Cover plates with significantly higher dead load stresses may have safety factors less than unity, which is a clear danger sign of fatigue susceptibility. When using 50% mean fatigue data, a safety factor range of 1.40 - 1.60 is recommended. A safety factor of 1.40 or greater takes material and load variations into account. When using the more conservative AWS fatigue categories for various weld details, a safety factor as low as 1.20 can be employed. In either case, safety factors less than 1.00 indicate serious potential fatigue problems.

8. FATIGUE DAMAGE TO BRIDGE COMPONENTS

A composite stress range-frequency histogram was developed by using the mean of each stress range and frequency of 15 bridges to indicate the susceptibility of main load-carrying members of bridges with particular details to fatigue damage. Of the 15 bridges studied, the peak stress range measured was only 5.5 ksi. This finding is similar to that of NCHRP 299,[3] which reports an effective stress range of 1-5 ksi. A stress range of 5.5 ksi affects only certain welded components listed as Categories D and E of the AWS Structural Welding Code, as shown in Figure 25a and 25b for redundant and non-redundant structures. For redundant structures, Category E weld details are the only ones affected by a peak stress of 5.5 ksi. Weld details susceptible to fatigue damage at 5.5 ksi include: (1) cover plates and larger plate-type attachments to girders; (2) ends of certain fillet-welded connections; (3) longitudinal stiffeners on girder webs; (4) plug welds and slot welds; (5) sharp changes in girder flange width or section; (6) cruciform weld joints. Other steel details not listed in AWS Categories D or E are not affected by a 5.5 ksi live load stress range.

Other non-welded designs of metallic main load carrying members were also examined for susceptibility to fatigue. Through an extensive series of fatigue tests, Fisher, Yen, Wang and Mann[16] established a threshold of 10 ksi as the minimum stress range needed to induce significant damage in new and existing riveted structures with and without holes, including both wrought iron and plain carbon steels. These S-N curves are shown in Figures 26-33.

Corrosion of major structural elements is another serious problem. Corrosion causes pitting, crevicing, and loss of load-bearing section. Corrosion can cause the fatigue rating of smooth girders to drop

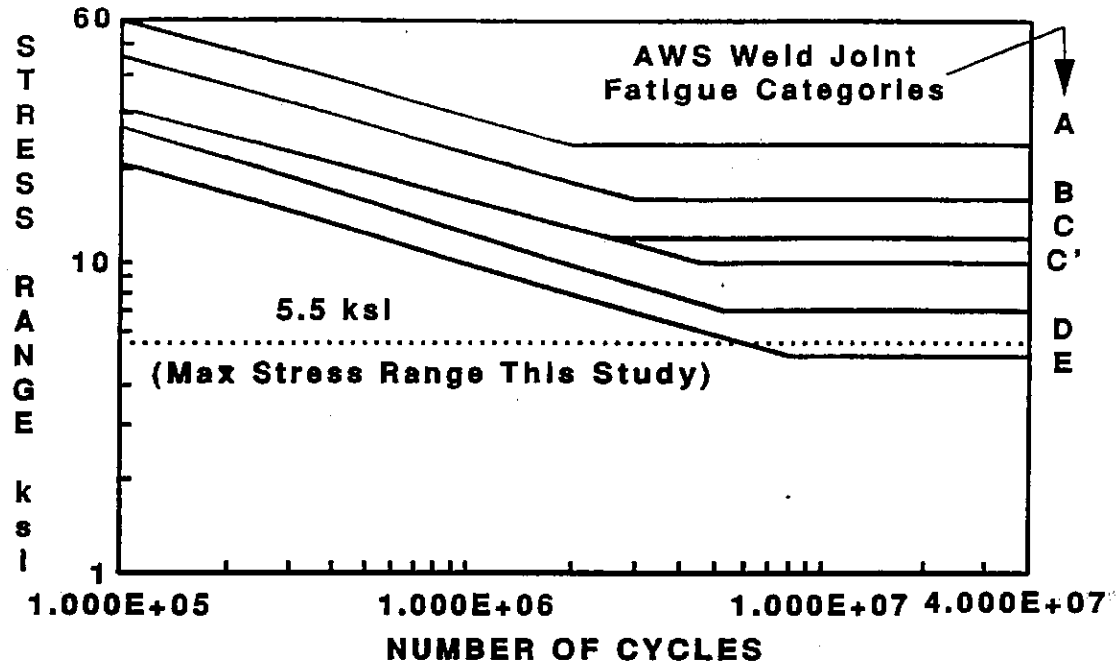

Figure 25a. AWS design stress vs. cycle life for redundant structures. Data Source: AWS Structural Welding Code ANSI/AWS D1.1, Miami, Florida.

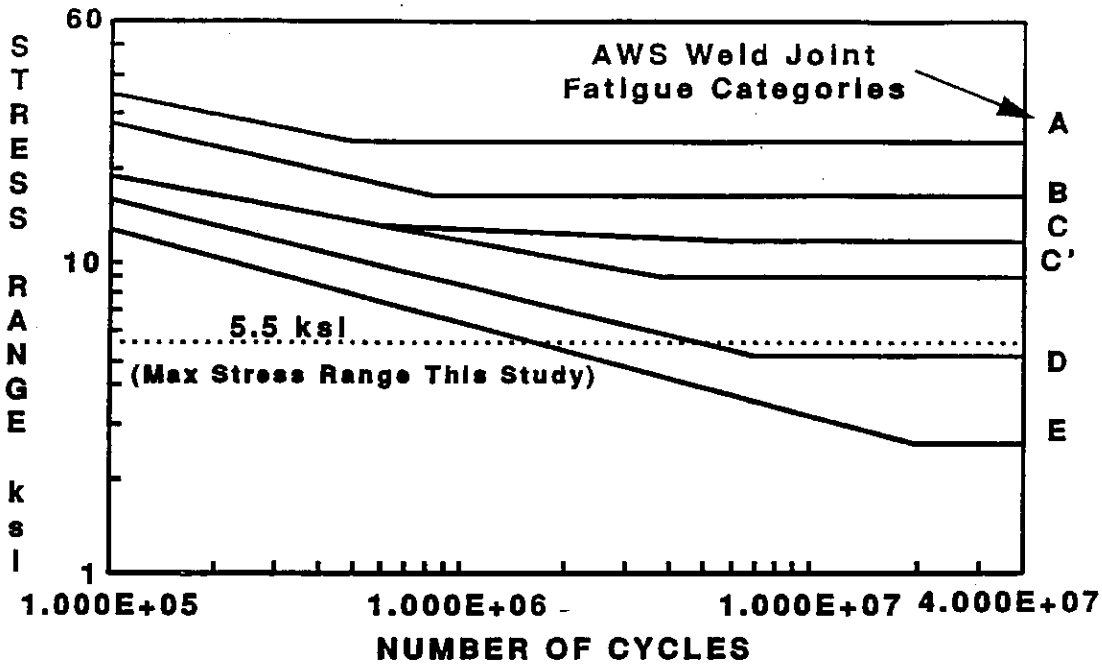

Figure 25b. AWS design stress vs. cycle life for non-redundant structures. Data source: AWS Structural Welding Code, ANSI/AWS D1.1, Miami, Florida.

significantly and can raise stress concentrations in members which will eventually form cracks. Albrecht, Shabshab, Li and Wright[17] took ASTM A 7 rolled carbon steel beams that had been exposed to the elements for 25 years and fatigued them to failure at various stresses. ASTM A 7 has a chemical composition and mechanical properties similar to ASTM A 36. They compared their results to smooth rolled sections in bending, which falls into AASHTO Fatigue Category A. Corrosion had reduced the fatigue resistance of smooth hot rolled beams to Category B or C. For ASTM A 588 weathering steels, pitting was deeper and more severe, particularly in steels that had been subjected to moist, sheltered exposures. Normally, the fatigue life of hot rolled, unpitted structural steel falls into ASTM A 588 Category A. If the ASTM A 588 steel is pitted, however, fatigue life is brought down by corrosion to Category E, which has an endurance limit of 7 ksi. This constitutes a three-fold reduction in fatigue strength. These results for ASTM A 7 and ASTM A 588 structural steels are shown in Figures 34 and 35.

Corrosion products can also cause major structural elements to be placed under additional strain by actual expansion. A typical example is the crevice corrosion exhibited by beams with riveted cover plates. The crevice corrosion causes the cover plate to expand and yield. Also, the rivets sustain additional shear and tensile stresses due to this cover plate expansion. Loss of section and penetration of rolled beams by corrosion pits can result in concentration of stresses in the corrosion holes, decreasing the time required for crack initiation.

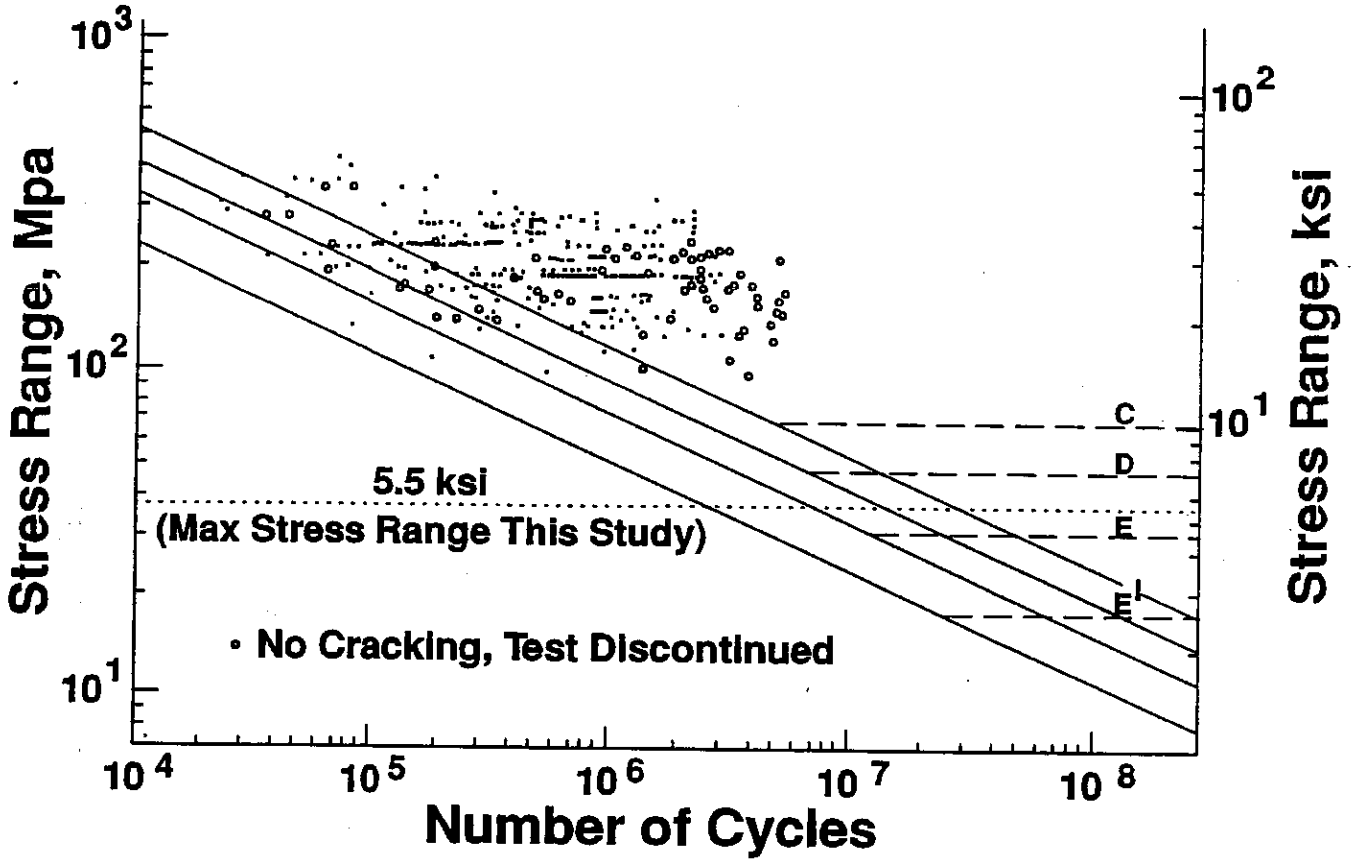

Figure 26. Fatigue resistance of riveted steel connections, specially fabricated for laboratory test. Data of Fisher, Yen, Wang, and Mann.

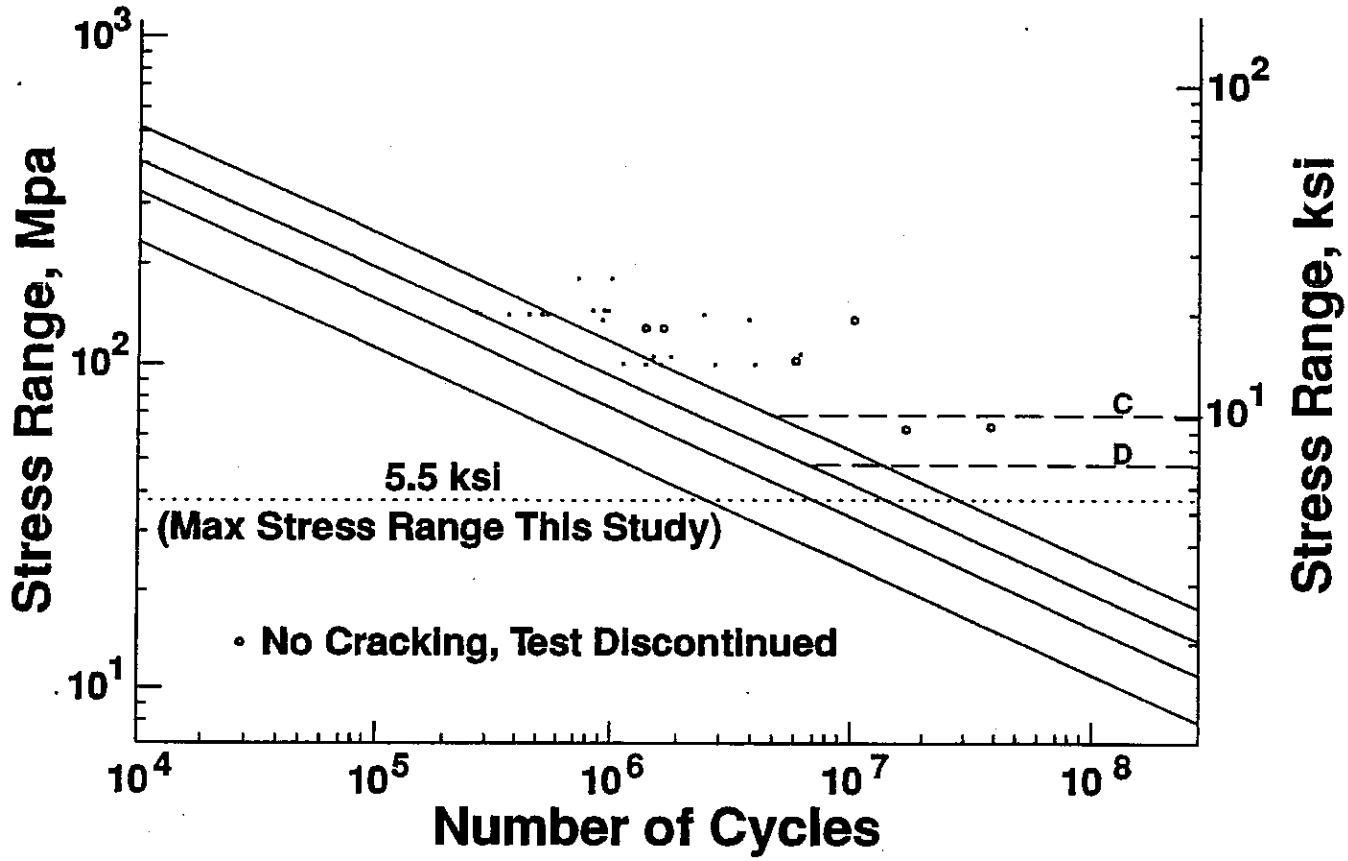

Figure 27. Fatigue resistance of riveted steel connections, fabricated from existing structures. Data of Fisher, Yen, Wang, and Mann.

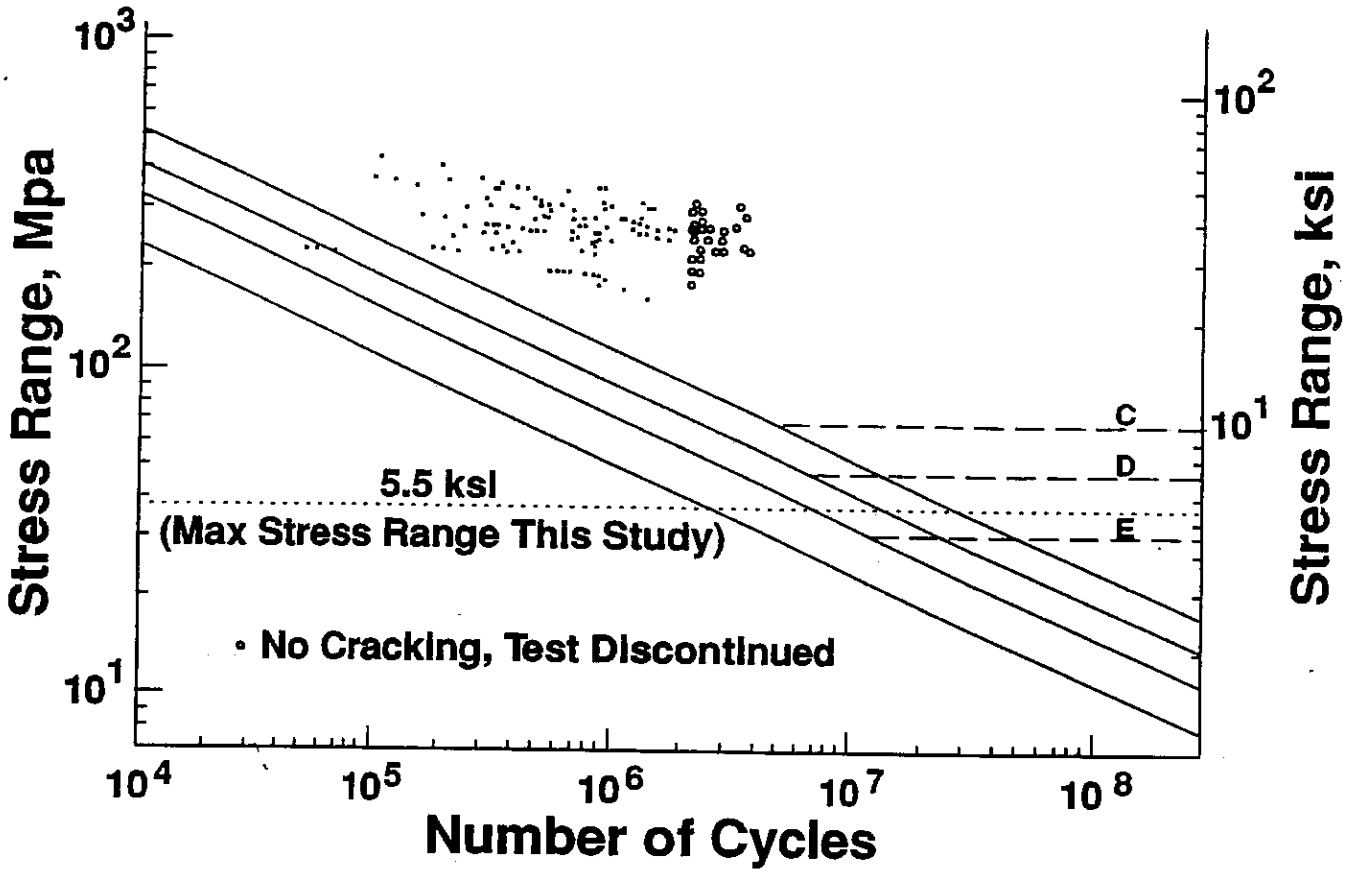

Figure 28. Fatigue resistance of steel plates with holes fabricated for laboratory tests. Data of Fisher, Yen, Wang, and Mann.

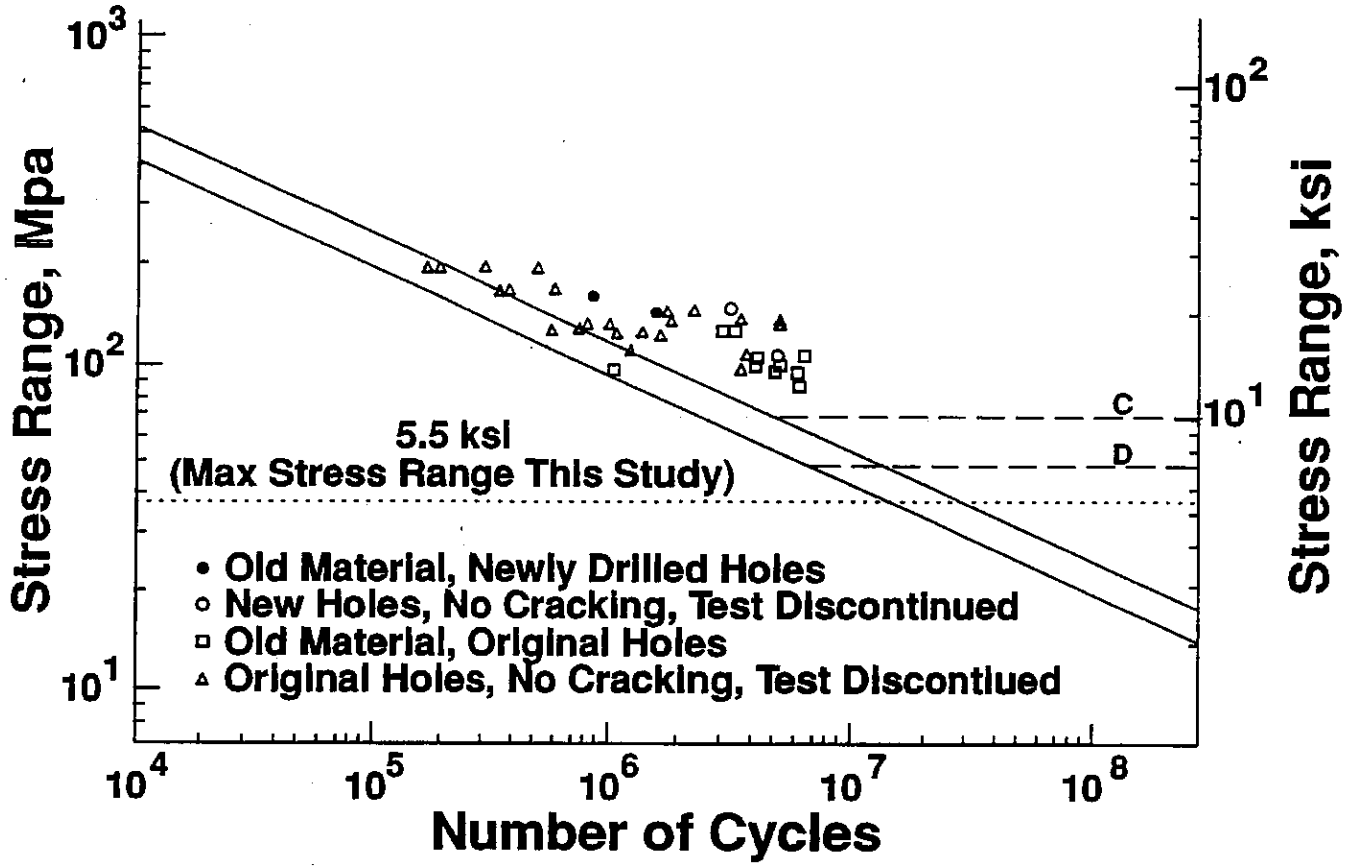

Figure 29. Fatigue resistance of steel plates with new or existing open holes, fabricated from existing structures. Data of Fisher, Yen, Wang, and Mann.

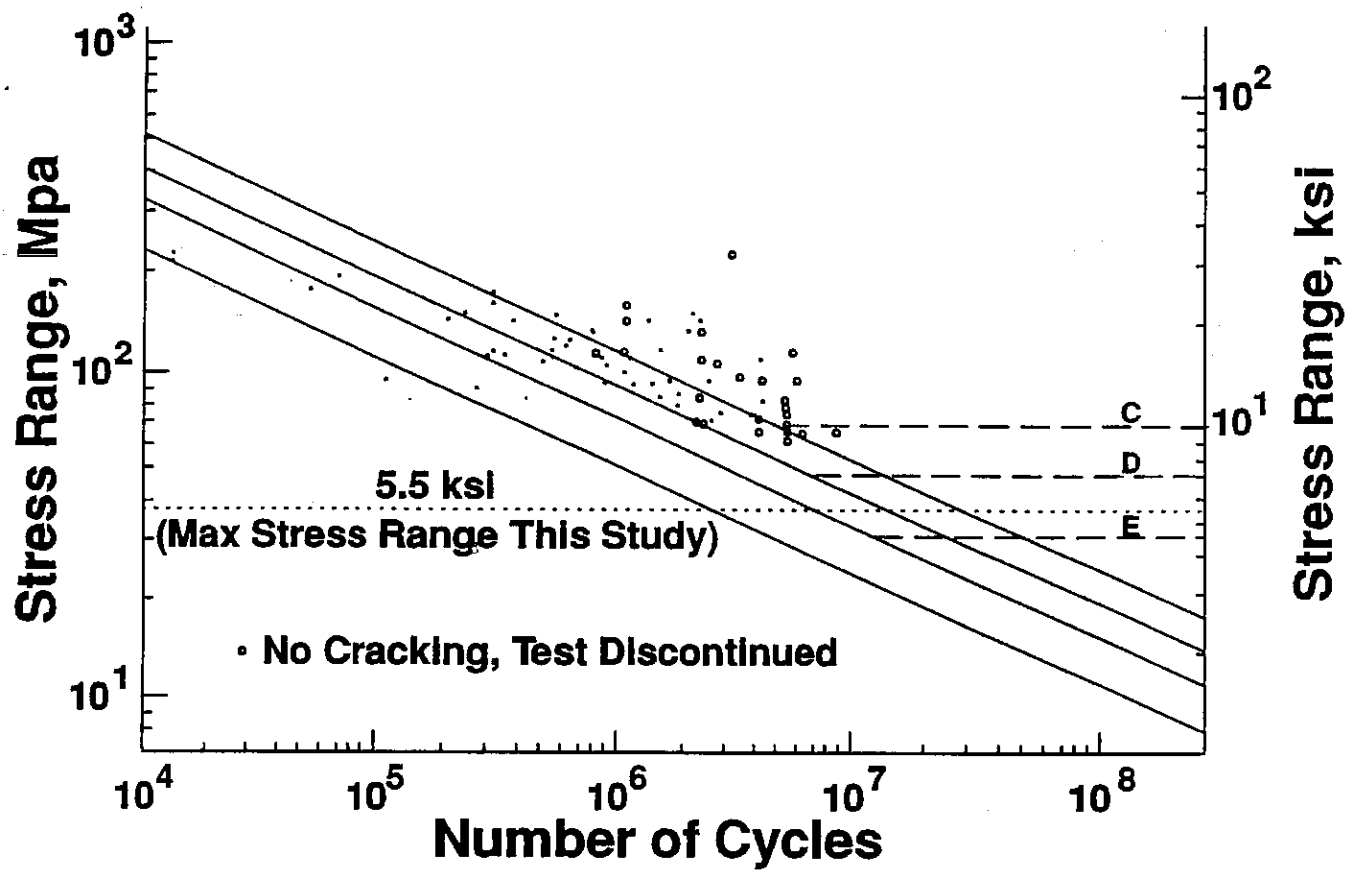

Figure 30. Fatigue resistance of wrought iron riveted connections. Data of Fisher, Yen, Wang, and Mann.

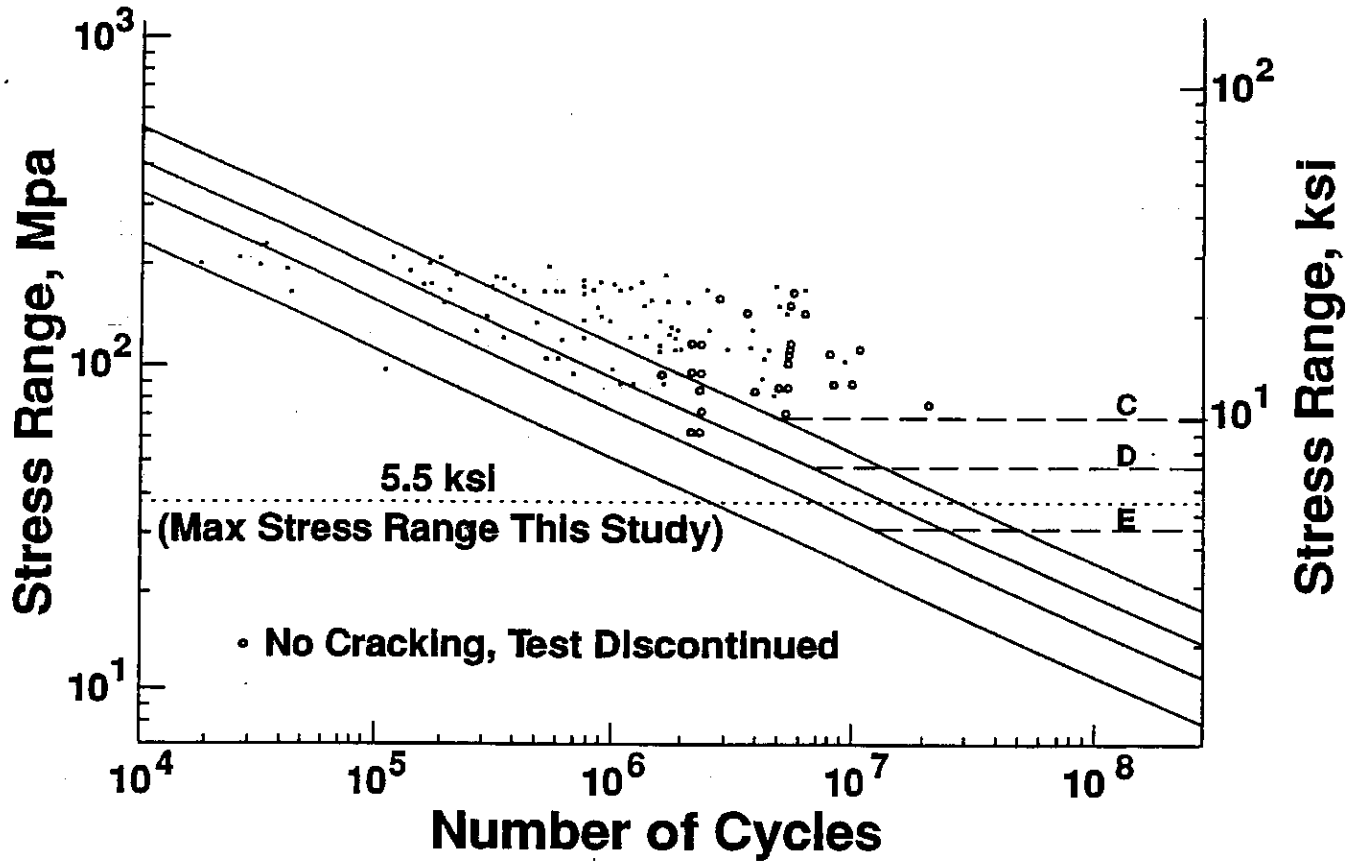

Figure 31. Fatigue resistance of wrought iron plates with open holes. Fatigue specimens were taken from truss bridge tension chord connections. Data of Fisher, Yen, Wang, and Mann.

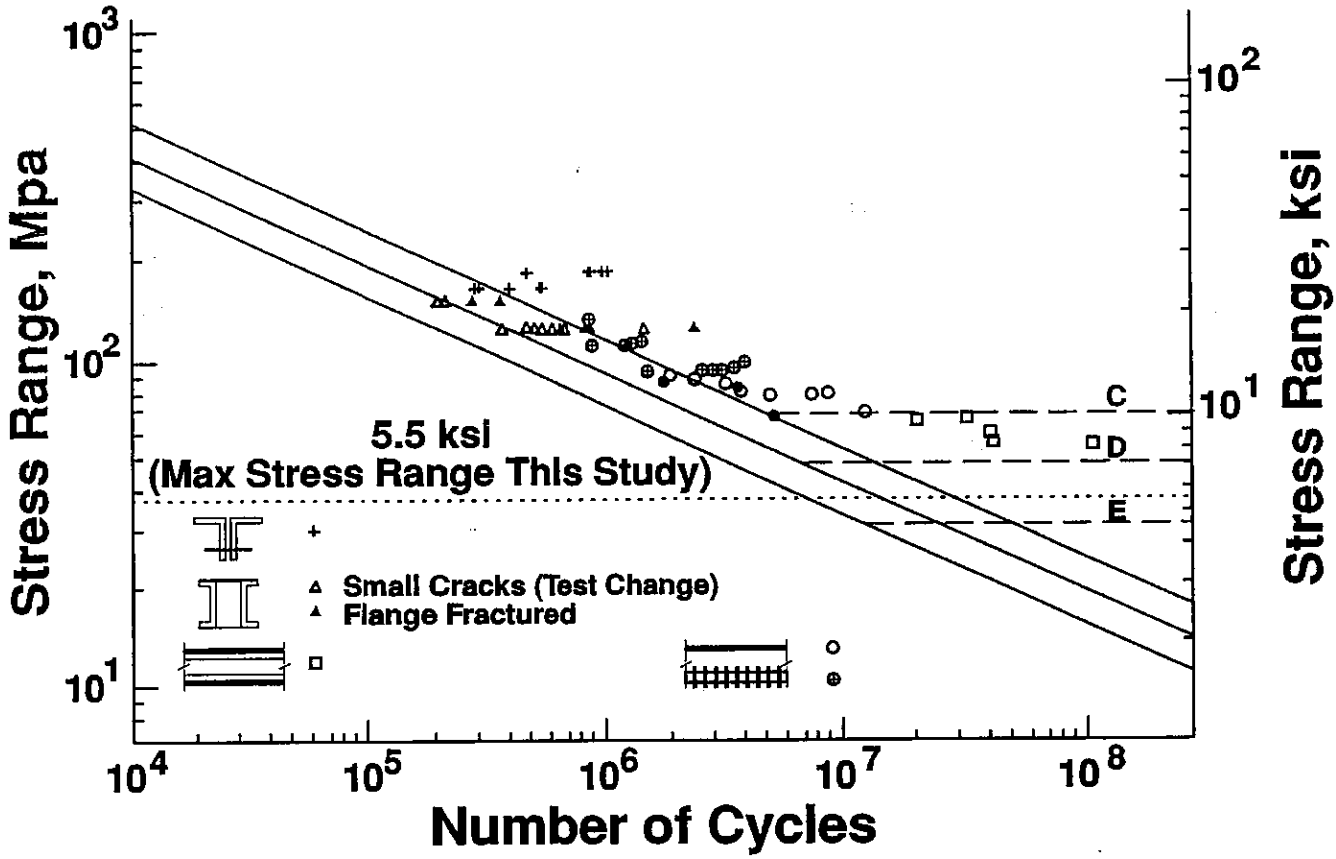

Figure 32. Fatigue test data for full scale numbers taken from riveted bridge structures. Data of Fisher, Yen, Wang, and Mann.

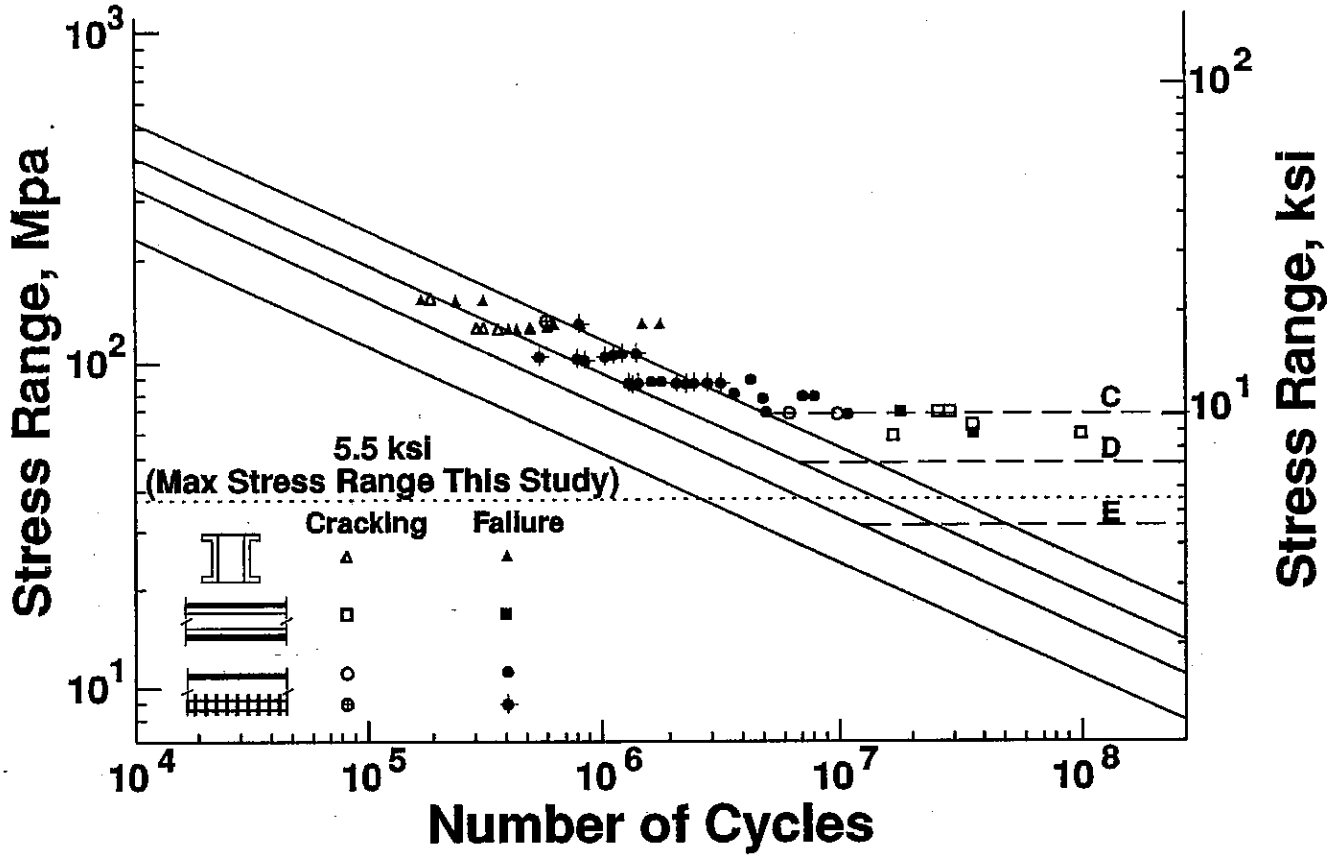

Figure 33. Comparison of first detectable cracking and failure of the sections of full-scale members. Data of Fisher, Yen, Wang, and Mann.

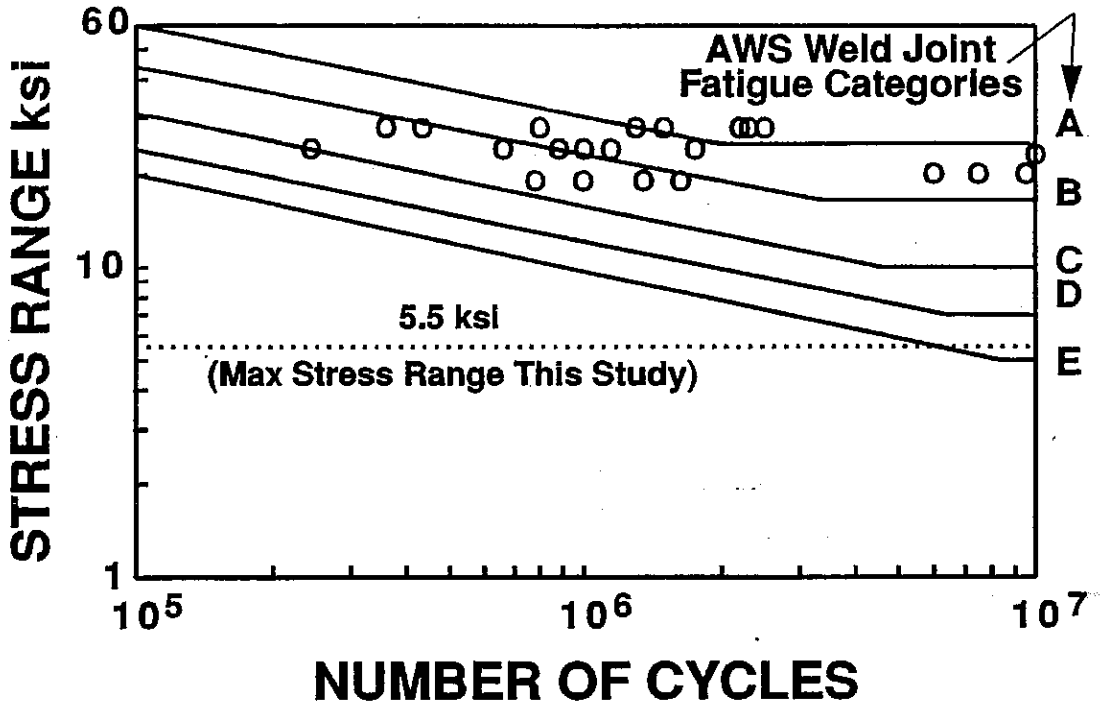

Figure 34. Fatigue test data for uncoated ASTM A 7 plain carbon steel beams exposed to Maryland weather for 25 years. Pits were rounded in this inland exposure. Plot based on data of Albrecht, et. al.[17].

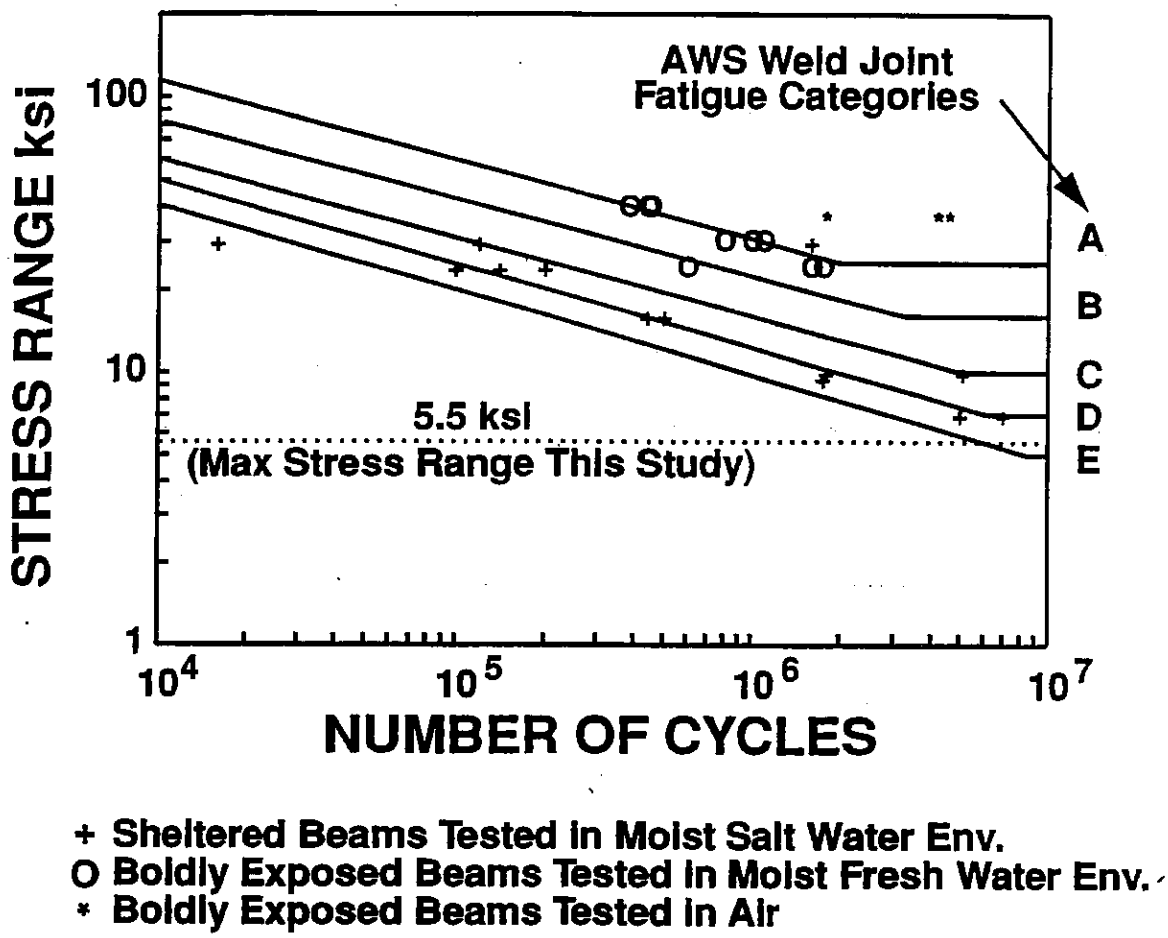

Figure 35. Fatigue test data for weathering steel beams exposed to air and moist atmospheres for 5.7 years. Plot based on data of Albrecht, et. al.[17]

Pitting was found by Albrecht and co-workers[17] to cause the severest reduction in fatigue life. Since pit depth is directly related to overall penetration, overall fatigue reduction factors can be directly derived from pit depths for structural and weathering steels, as shown in Figures 36 and 37. Pits 4-5 mm deep are able to magnify fatigue stresses by a factor between 2 and 3. These findings are particularly related to rolled sections in tension or bending that have sustained severe pitting or actual penetration at (1) the web-flange interface, (2) at the underside of the lower flange, (3) in gusset plates, or (4) in rolled angles. These four structural locations or elements are particularly susceptible to fatigue damage when peak stress ranges are 5.5 ksi or slightly greater.

Tests of reinforced concrete slabs in air indicated an endurance limit of approximately 20 ksi in the reinforcing bars, with a fatigue ratio of 0.5 (endurance limit/tensile strength). This ratio value of 0.5 is typical for plain carbon steel fatigue-tested in air. These results are shown in Figures 38 and 39. However, the fatigue ratio 0.5 no longer holds true when the reinforced concrete is severely cracked due to freeze-thaw and salt application.

Post-tensioned concrete beams also are not apparently at risk even with the fretting of cable strands in metal ducting, as shown in Figure 40. The threshold of damage to fretted post-tensioned cables is approximately 12 ksi at 10,000,000 cycles.

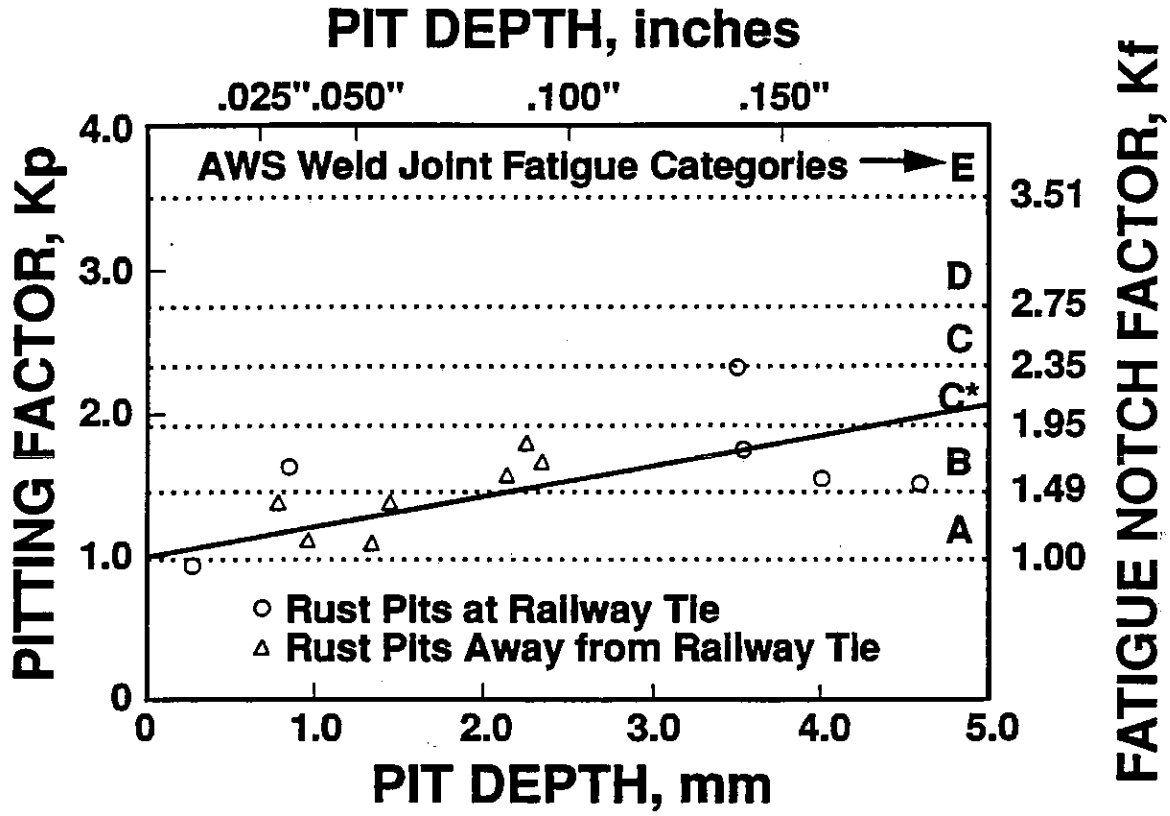

Figure 36. Pitting Factor for carbon steel beams. Pits in plain carbon structural steel are generally rounded. Data of Albrecht, et. al.[17]

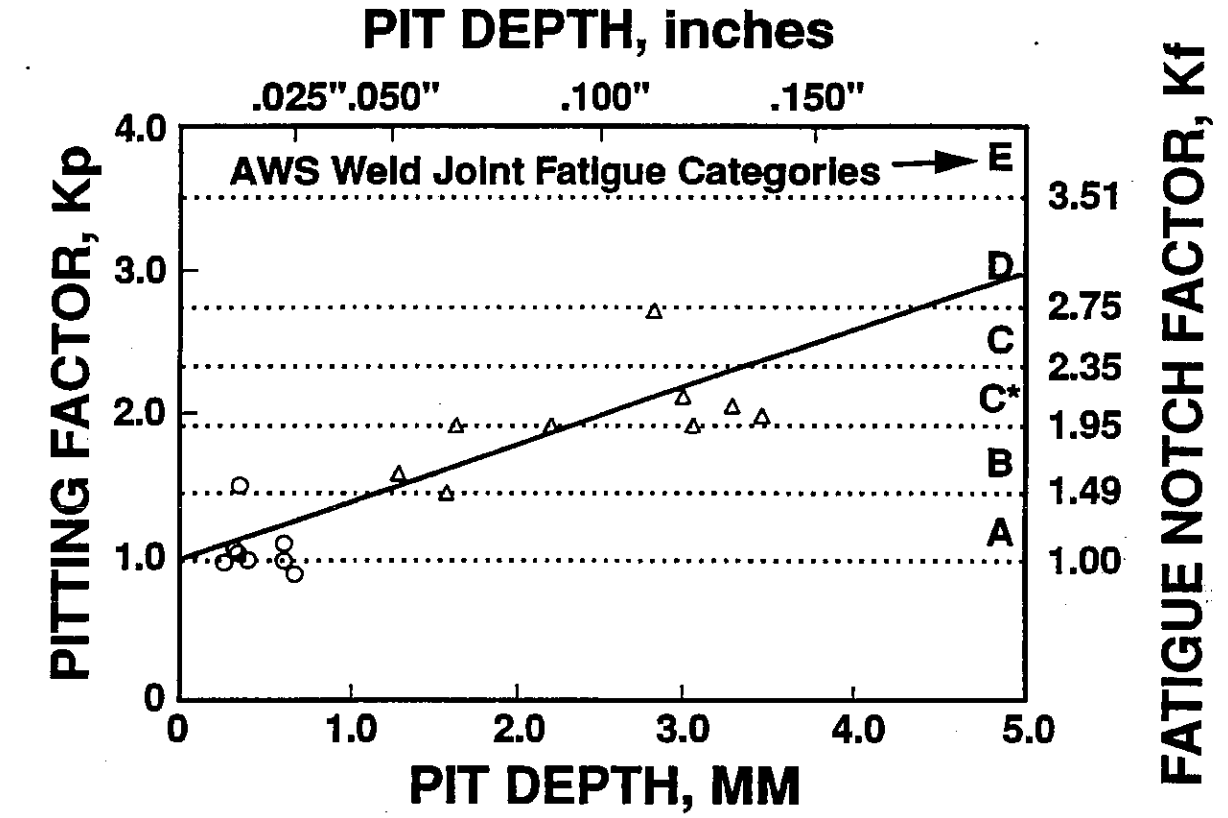

Figure 37. Pitting Factor for ASTM A 588 weathering steel beam. Pits in structural steels containing substantial levels of copper, phosphorus and chromium are generally deeper than in conventional structural steels. Data of Albrecht, et. al.[17]

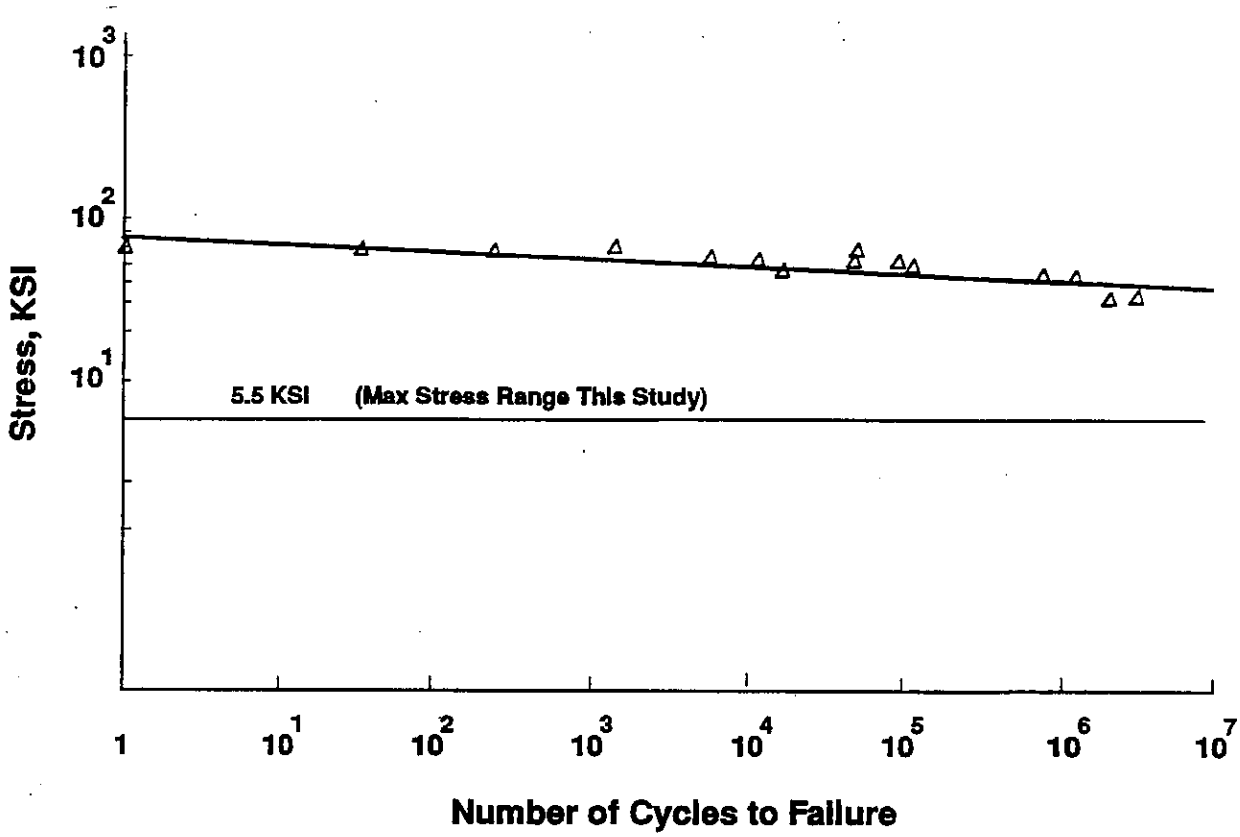

Figure 38. Fatigue of orthotropically reinforced concrete deck slabs in air only. ASTM A 615 Grade 40 rebars (70 ksi UTS minimum, 40 ksi YS minimum). Data of Batchelor, Hewitt, and Csagoly.

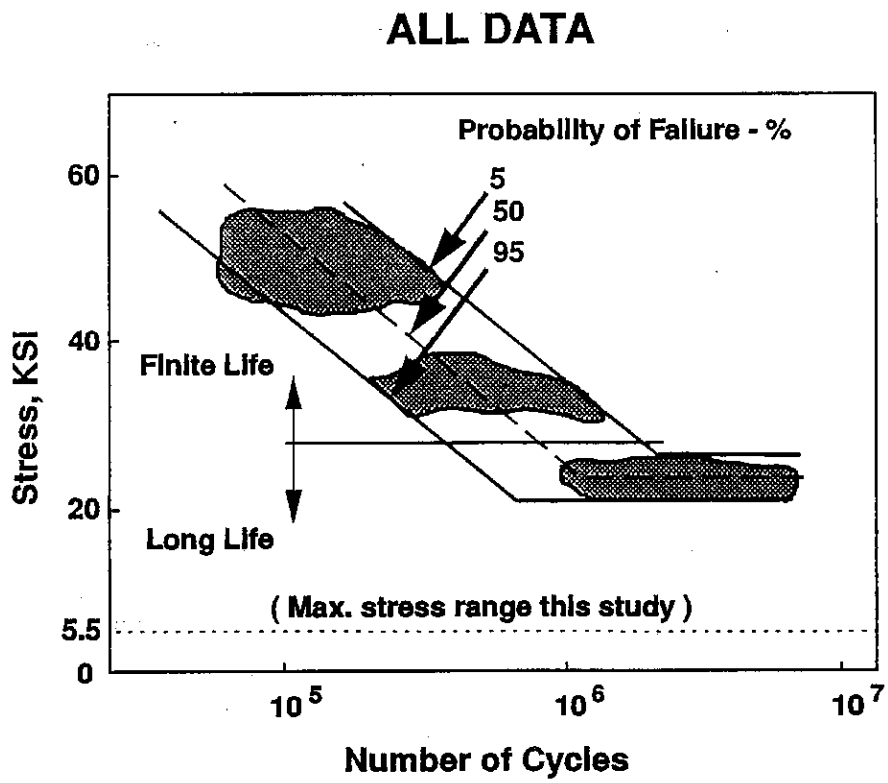

Figure 39. Fatigue life of uncorroded straight deformed bars. Data of Portland Cement Association.

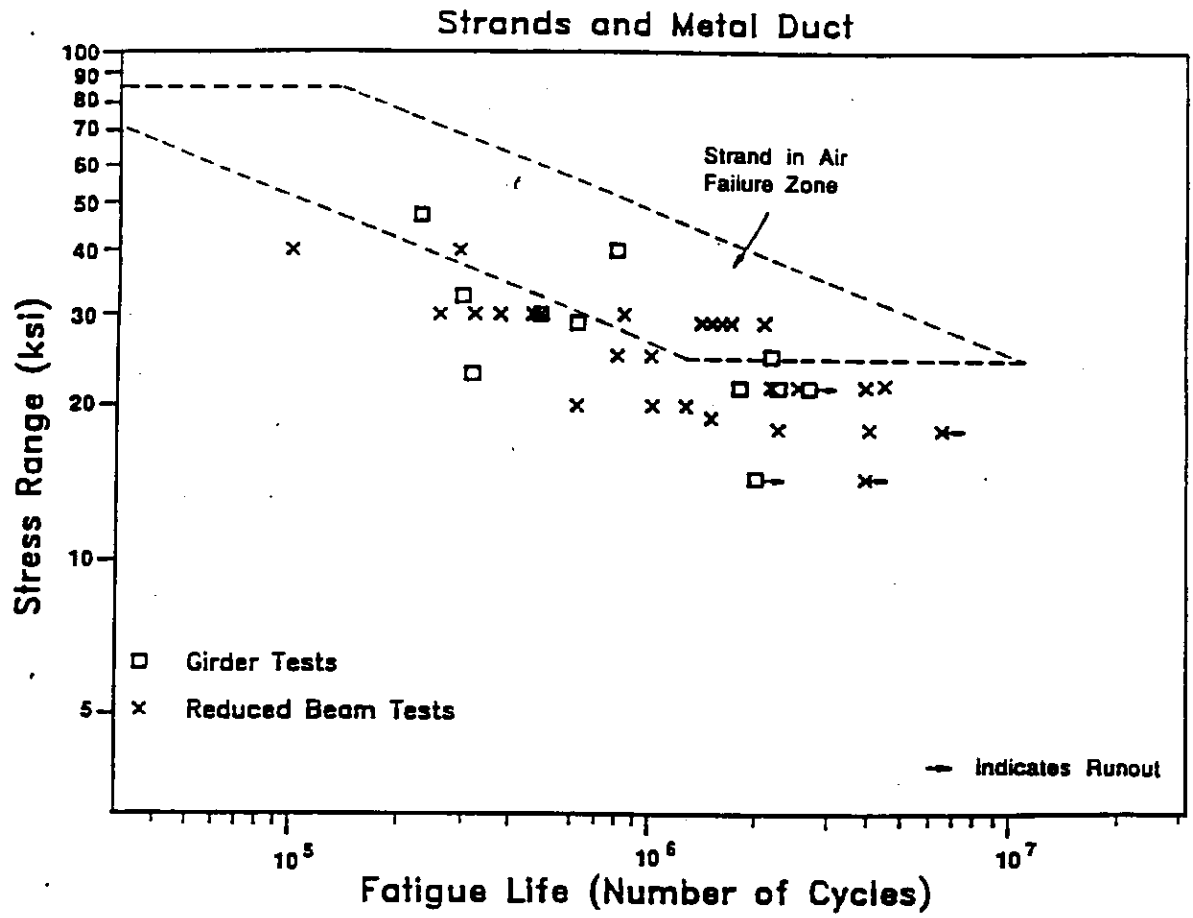

Figure 40. Detrimental effect of fretting fatigue on strands in metal duct. Data of Wollman, Yates, Breen, and Kreger.

9. BRIDGE DECK DETERIORATION

A typical bridge deck is a periodically jointed, transversely continuous slab of reinforced concrete, varying in thickness from 6 to 8 inches. In comparison, this 6 to 8-inch thick deck is supported by a far more rigid superstructure whose girders or reinforced concrete beams may typically range from 24 inches to 72 inches in depth. The reinforced concrete deck is essentially a dead load which absorbs the wheel contact stresses from live loads passing over the bridge. Considering reinforced concrete as a composite material, it has a brittle matrix with little capacity for impact absorption and ductility. In contrast, its reinforcing bars are the relatively more ductile elements or fibers. If the brittle matrix becomes discontinuous by fragmentation into smaller discrete elements, the ductile overlapping bars lose their development and thereby sustain losses in both tensile and shear capacity and cease to be an integral structural element.

There are several causes for the formation and propagation of cracking and the subsequent discontinuity of reinforced concrete in bridge decks. Many micro and macro-cracks are formed after concrete placement which originate from shrinkage due to improper curing and rapid drying. Premature construction or traffic loads may also induce cracking. Because concrete has a long curing time, it does not achieve full strength until months have elapsed, although it may quickly achieve minimum compressive strength based on the testing of cores, cured cylinders, or beams poured from the same batch as the deck. Concrete is also subject to freeze-thaw damage in climatic regions where temperatures frequently drop below 32° F. Where freezing conditions involve snow and ice, salt application can cause

electrolyte intrusion. Because of the inhomogeneity of concrete and micro-cracking, local-action corrosion cells establish themselves, leading to corrosion of the rebars. The expansion of the corrosion products of iron causes spalling and disbonding of the concrete. Preliminary studies by Japanese investigators[18] showed that when water flowed onto reinforced concrete beams subjected to cyclic loading, failure was accelerated. Fatigue lives were reduced by approximately one order of magnitude. The proposed mechanism of failure in their analysis was the formation of crack surfaces which were purged of cementitious debris by the pulsating and pumping action of water induced by cyclic deflection and vibration. Without water, such debris would remain in the cracks and the cracks would not be able to open up as quickly and thereby propagate.

Another study of corrosion fatigue of reinforced concrete conducted by British investigators[19] showed that seawater did not degrade fatigue life, but that 3.5% sodium chloride or plain tap water were detrimental. This phenomenon was attributed to deposition of seawater salts in the cracks of the concrete. Fatigue failure was also more pronounced at 5 Hz. vs. 0.17 Hz. Higher loading frequencies presumably decrease the ability of seawater salts to form deposits in cracks. Crack sites in the concrete were also locations where corrosion of the rebar was particularly active.

10. COMPARISON OF FATIGUE LIFE ESTIMATION PROCEDURES

This chapter compares and contrasts three methods for estimating the expected fatigue life of Category E welded details. The methods used were: 1) the new histogram-linear damage rule as described in this report, 2) a root mean cube equivalent stress range-linear damage rule as described by Barsom and Rolfe[20], and 3) procedures given in NCHCP 299 Appendix A (Equation (1) in this report). The root mean cube equivalent stress range and the NCHRP 299 procedures are currently the two most popular bridge fatigue calculation methods used in the United States.

Six bridges with welded coverplates were used for this comparison. The prior historical fatigue damage sustained by each of these bridges was not taken into account. No growth in traffic was also assumed in the following comparisons.

Method 1

Using the linear damage rule in a straightforward, incremental fashion, the number of cycles per day for each stress range was multiplied by 365 to represent a histogram for a year-long loading block. The total fraction of life consumed in the weld after one year of traffic was then calculated by comparing the number of available stress cycles for that stress range for a particular detail, as shown in the example in Chapter 4. Since this is the damage fraction for one year, the expected fatigue life is calculated from

$$L = \frac{1}{D} \qquad (7)$$

where: L = expected fatigue life, years
D = fraction of life consumed in one year.

Method 2

A modified method using the linear damage rule is presented by Barsom and Rolfe.[20] The main difference between this method and the histogram method is the assumption that a calculated equivalent stress range will accurately represent the entire histogram. This equivalent stress range, which is a root mean cube statistical approximation, is used to calculate the number of equivalent cycles to failure. The damage fraction is the ratio of total cycles to the number of equivalent cycles to failure. The equivalent stress range is given by:

$$S_r = \left[\left(\sum_{i=1}^{m} a_i \Delta\sigma_i \right)^3 \right]^{1/3} \qquad (8)$$

where: $a_i = \dfrac{n_i}{\Sigma N_T}$

n_i = number of stress cycles at a particular stress level S_i

ΣN_T = total number of stress cycles in the entire histogram

$\Delta\sigma_i$ = stress range, ksi.

m = number of increments of stress cycles

Using this value for S_r in (4), the equivalent number of cycles to failure, N_f, is calculated. The fatigue damage is then:

$$D = \frac{N_f}{\Sigma N_T} \qquad (9)$$

where: N_f = total available number of cycles at the root mean cube equivalent stress for a particular N-S equation for a specific detail.

The expected fatigue life is calculated from (7). The drawback of the root mean cube method is that it does not represent distributions well where permit and non-permitted overloads are frequent since these distributions are often skewed or abnormal.

Method 3

This method uses the formula for finite remaining life which is introduced in NCHRP 299 Appendix A. The traffic volume was calculated using the commerical ADT and the lane factor given in Section 6.3.5 for each particular bridge. The equivalent stress range, S_r, is the same as calculated for Method 2.

The results of all three methods are shown in Table 9. The expected fatigue lives for each bridge are high for both 50% mean fatigue data and the use of higher reliability AWS fatigue categories. The expected fatigue life is reduced by 2/3 when redundant AWS fatigue category E is used in the calculations instead of 50% mean fatigue data.

Table 9 shows wide discrepancies in the calculated expected fatigue lives between the three methods. In all cases, and by substantial margins when using mean data, the NCHRP 299 procedure produced the most conservative results (has lowest expected life). The average difference between the two linear damage methods was 7.7%, with the direct histogram-linear damage method (Method 1) producing slightly more conservative estimates. The Palmgren-Miner linear damage rule has been shown to be a reasonably accurate and straightforward predictor of fatigue life for structures[21].

Therefore, it is noted that the root mean cube method errs slightly to the non-conservative side while the NCHRP 299 procedure errs significantly to the conservative side. Such conservatism is expected, of course, from the NCHRP 299 design procedure which can be applied to all types of bridges. However, when analyzing existing bridges, such a high level of conservatism may predict early failure (crack initiation) when the reality may be far different.

In terms of calculation effort, Method 1 was the easiest to follow and the fastest. Method 2 required additional time and effort, and Method 3 took the longest. The speed and relative accuracy of the histogram-linear damage method are due to its straightforward calculation procedure and its use of actual strains. There are no statistical measures or empirical parameters to be identified and it uses stress range-frequency data taken directly from an actual bridge in question. The methods of NCHRP 299 may be useful for generalizations or for conservative design purposes where actual histograms are not available. However, Table 9 shows that the use of fatigue life estimation procedures which rely on broadbrush loading factors results in loss of accuracy since they are approximations only, and are not derived from actual measurements.

A clear picture that emerges from this study is that fatigue of steel bridges is not significant when traffic is moderate and stress ranges are less than 3 ksi, even when cover plates are involved. Fatigue is problematic when traffic is continually increasing in volume and truck weights are progressively rising or their overloads are not monitored. Even when 50% mean data is not used, the reliability of existing steel super structures is made patently evident, and only their functional deficiencies or corrosion problems will render them obsolete.

TABLE 9

COMPARISON OF VARIOUS FATIGUE LIFE ESTIMATION PROCEDURES[a]

Expected Fatigue Life of Detail in Years

	Method 1 (histogram-linear damage)		Method 2 (equiv. stress-linear damage)		Method 3[c] (NCHRP 299)	
Bridge[b]	AWS[d]	mean[e]	AWS[d]	mean[e]	safe[d]	mean[e]
0160335	130	369	137	416	120	240
(4350)			S_r = 1.74 ksi		c = 1.0, F_L = 0.4	
1010019	424	1,243	443	1,342	314	627
(900)			S_r = 1.63 ksi		c = 1.5, F_L = 0.6	
0720014	518	1,569	524	1,640	459	917
(550)			S_r = 1.45 ksi		c = 1.5, F_L = 0.6	
0420017	1,918	5,845	1,977	6,170	1,781	3,562
(375)			S_r = 1.40 ksi		c = 1.0, F_L = 0.6	
0650005	808	2,282	839	2,514	1,316	2,632
(200)			S_r = 1.91 ksi		c = 1.0, F_L = 0.6	
0540031	26,385	82,645	26,990	86,694	5,254	10,508
(125)			S_r = 1.23 ksi		c = 1.5, F_L = 0.6	

[a] Based on actual average daily histogram data extrapolated to 365 days, with no traffic growth, and for Category E welded details only.

[b] Numbers in parenthesis are commercial ADT values.

[c] f=1.0 or 2.0, K = 1.1, for all cases. F_L is the lane factor, c is the number of stress cycles per truck passage.

[d] Uses AWS Structural Welding Code Fatigue Category E for redundant structures as a basis for life determination.

[e] Uses Ship Structures Committee 50% mean fatigue data for life determination.

11. EFFECT OF PERMIT LOADS ON ACCURACY OF DAMAGE CALCULATIONS

A clear cut example of the difference in the accuracy of the equivalent stress-linear damage method vs. the histogram-linear damage method occurs when a bridge sustains a substantial number of permit loads over and above the legal limit of 80,000 lbs. Using data gathered for the entire month of August 1992, all permit loads granted involving the use of US 45 were reviewed to see if they passed over Bridge 0160335 which crosses the rail yards in Franklin Park on Mannheim Road near O'Hare Airport. This voluminous printout (280 pages) was scanned for all loads above 80,000 lbs, ranging from the transportation of heavy cranes, presses, machine tools, to backhoes, etc. Loads above 80,000 lbs were linearly proportioned to increase the stress range in the bridge by the following relationship:

$$S_r = S_{80}\left[\frac{L-80{,}000}{80{,}000} + 1.0\right] \qquad (10)$$

where: S_r = stress range in Bridge 0160335 with permit load

S_{80} = stress range at 80,000 lbs legal load; for Bridge 0160335, stress range is 5.5 ksi

L = gross weight of load above 80,000 lbs.

A seperate experimental confirmation of the above equation (10) was undertaken. An interstate bridge (independent of the 15 bridges in this study) subjected to a heavy permit load was instrumented, and the resultant strain readings obtained indicated that the stress range increased in linear proportion for loads above 80,000 lbs. The bridge was located on I-80 over the Burlington Northern RR near

Ottawa, Illinois, and is a three span, 5-girder continuous, 36 inch deep rolled wide flange bridge which carries a heavy volume of daily truck traffic. Main girder strain data at the 80,000 lb load levels indicated an average stress range of 3.5 ksi, whereas the main girders sustained a measured stress range of 12.3 ksi for a 313,000 lb. permit load. Perfect proportionality of loading would result in a stress range of 13.8 ksi. Indicated error was therefore -10.7%, which is quite close to linear proportionality, considering the normal variations encountered in stress ranges measured in steel bridges.

Since Bridge 0160335 (US45/Mannheim Rd.) was originally sampled without registering the passage of any permit loads, 5.5 ksi was determined to be the maximum stress range for legal loads. The resulting new permit load stress ranges calculated by equation (10) were then counted for frequency throughout the month of August. For convenience to illustrate the projected damage effects, the permit loads and legal loads were multiplied by 12 and put into a yearly basis, as shown in Figure 41.

Using the data plotted in Figure 41, a comparison chart between the root mean cube-equivalent stress method vs. the histogram-summation method is shown in Table 10. In the equivalent stress method, the proportional damage of each stress range is multiplied by the cube of the stress range. Each of these sums is added up and the cube root of this cumulative value results in an equivalent stress range that supposedly represents all the stress events. For Bridge 0160335, this equivalent stress is 1.79 ksi. Most of the lighter vehicular activity is concentrated around this stress range, but the more significant damage is actually sustained by passage of heavier vehicles. The drawback of the

equivalent stress method is that it assigns substantially lower values to damage events caused by heavy vehicles, especially permit loads. The lifetime predicted by the equivalent stress - linear damage method for Bridge 0160335 is 372 years.

In contrast, the histogram-summation method compares damage in a direct, linear fashion. Each individual damage at a specific stress range is referenced to its respective available life at each stress range, not by a generalized equivalent stress. Because histogram summation puts emphasis on each stress range, heavier vehicles are counted in more direct proportion to the damage they cause to the bridge and to its various fatigue-susceptible details. For example, the equivalent stress damage at 2 ksi stress range is 0.672, and at 8.0 ksi is 0.241. The ratio of heavy-to-light damage is .241/.672 = 0.359 for the equivalent stress method. By comparison, the histogram-linear damage method sustains a damage of 0.00032 at 2 ksi and .00017 at 8 ksi, resulting in a heavy-to-light damage ratio of .00017/.00032 = 0.500. The histogram-linear damage method results in more emphasis on damage from heavy trucks even though their statistical population is considerably less than the bulk of traffic. The histogram-linear damge method predicts an estimated life for Bridge 0160335 at 298 years, which is 25% less than that predicted by the equivalent stress method.

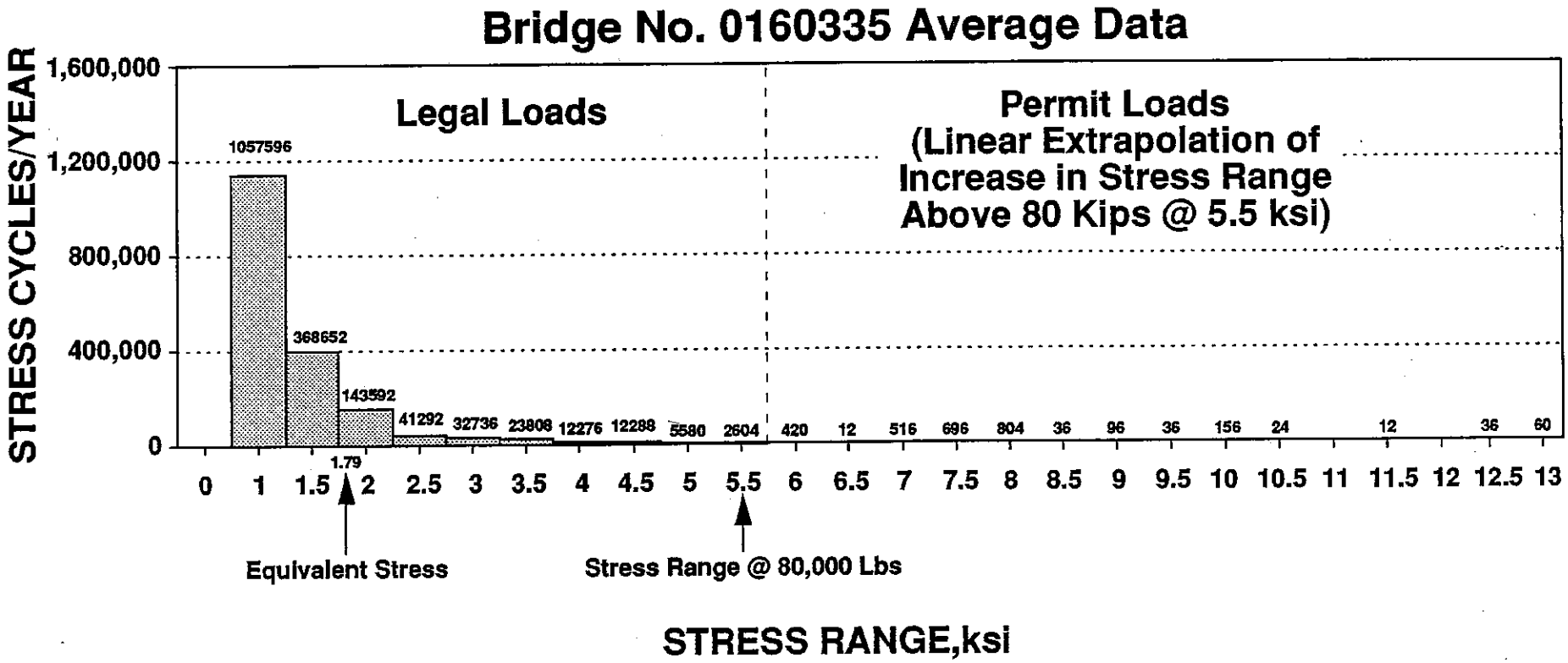

Figure 41. The number of stress cycles at 0.5 ksi increments for legal loads to 5.5 ksi and permit loads above 80,000 for Mannheim Rd. Bridge (US 45) near Franklin Park, IL, south of O'Hare Airport.

TABLE 10

COMPARISON OF EQUIVALENT STRESS VS. HISTOGRAM - LINEAR DAMAGE ESTIMATES FOR BRIDGE 016-0335

No. of Stress Cycles	Equivalent Stress Method				Histogram-Linear Damage	
Per Year	$\Delta\sigma$	$\Delta\sigma^3$	$\Sigma\frac{n_i}{N}=\alpha$	$\alpha[\Delta\sigma]^3$	available cycles, N_{sri}	$\frac{n_i}{N_{sri}}$
1057596	1	1	.621	.621	4.22×10^9	.00025
368652	1.5	3.375	.216	.729	1.13×10^9	.00033
143592	2	8	.084	.672	4.42×10^8	.00032
41292	2.5	15.6	.024	.374	2.14×10^8	.00019
32736	3	27	.019	.513	1.18×10^8	.00028
23808	3.5	43	.014	.601	7.14×10^7	.00033
12276	4	64	.007	.448	4.62×10^7	.00027
12288	4.5	91.1	.007	.638	3.15×10^7	.00039
5580	5	125	.003	.375	2.23×10^7	.00025
2604	5.5	166	.0015	.250	1.64×10^7	.00016
420	6.0	216	.00025	.054	1.23×10^7	.00003
12	6.5	275	.000007	.002	9.51×10^6	-
516	7	343	.0003	.103	7.47×10^6	.00007
696	7.5	422	.0004	.169	5.97×10^6	.00012
804	8.0	512	.00047	.241	4.84×10^6	.00017
36	8.5	614	.00002	.012	3.97×10^6	-
96	9	729	.000056	.041	3.30×10^6	.00003
26	9.5	857	.000021	.017	2.76×10^6	-
156	10	1000	.00009	.090	2.34×10^6	.00007
24	10.5	1158	.000014	.016	2.00×10^6	.00001
12	11.5	1520	.000007	.002	1.48×10^6	-
36	12.5	1953	.00002	.039	1.13×10^6	.00003
60	13	2197	.000035	.077	9.96×10^5	.00006
1,703,328 = N_t				$\sqrt[3]{5.784} = \Delta\sigma_{rms}$		.00336 = D

NOTES (for Table 10)

(1) Equivalent stress for Bridge 0160335, including permit overloads, is

$\Delta\sigma_{rms} = [\Sigma\alpha_i \ (\Delta\sigma_i)^3]^{1/3} = [5.784]^{.333} = 1.79$ ksi

Life estimate = N_f/N_t $\quad N_t = 1{,}703{,}328$ cycles;

$N_f = 4.218 \times 10^9 \ (S)^{-3.256}$; $S = 1.79$ ksi; $N_f = 6.28 \times 10^8$ cycles

Life estimate = 372 years

(2) Histogram - linear damage life estimate = 1/D

D = damage per year where $D = \Sigma \frac{n_i}{N_{sri}} = .00336$

D = 1/0.00336 = 298 years.

12. SUMMARY

The load spectra of 15 bridges of various design throughout the State of Illinois were analyzed to determine a rapid means of assessing fatigue damage. Critical fatigue details in the superstructure of the bridge were instrumented with strain gages, and the stress range-frequency data for these details were gathered and processed using a rainflow cycle counting algorithm. The resulting stress range-frequency histogram was then used to calculate the number of stress damage events incurred by the traffic passing over the bridge. Because the histogram is representative of daily traffic, each stress range frequency can be multiplied by the number of days in the design life or anticipated future life of the bridge. Traffic growth and increased truck weights can also be incorporated by adjusting the individual histogram stress ranges and/or frequencies upward on an annual or projected basis. This method gives a direct, accurate and quantifiable assessment of superstructure damage in specific structural details without resorting to indirect analytical methods. An equation for calculating the factor of safety for a fatigue-prone detail was developed based on the Gerber parabolic relationship. The new modified equation incorporates the actual fatigue strength of specific details and the live load stress range in addition to mean stress effects.

The actual change in measured stress range for a multigirder bridge due to a gross vehicle weight change from a nominal 72,000 lbs. (72,350 actual) to 80,000 lbs. (81,700 actual) was measured by the use of strain gages. Results showed that approximately a 1:1 direct

relationship exists between percent weight increase and percent stress range increase for multi-girder bridges.

A review of the literature was conducted in which non-welded designs of metallic and reinforced concrete main load carrying members were examined for susceptibility to fatigue. These designs included new and existing riveted structures with and without holes, including both wrought iron and plain carbon steels, reinforced concrete slabs tested in air, and post-tensioned concrete beams. Different types of steel, specifically ASTM A 7 and ASTM A 588, were examined for reduction in fatigue resistance due to corrosion. Pitting was found to cause the severest reduction in fatigue life, especially in ASTM A 588 weathering steels. In reinforced concrete, it was found by Japanese investigators[18] that water flowing onto beams subjected to cyclic loading reduced fatigue life by approximately one order of magnitude compared to beams fatigued in air.

The histogram-linear damage procedure detailed in this report was compared with the root mean cube-linear damage rule procedure and the indirect, empirical methods given in NCHRP 299. The comparison showed that the histogram-linear damage rule procedure discussed herein gave results that were the most direct and straightforward. The NCHRP 299 method produced highly conservative results. The histogram-linear damage procedure was the fastest and easiest to calculate, and took permit and nonpermit overload events into account on a precise basis compared to the other less accurate statistical methods.

13. CONCLUSIONS AND RECOMMENDATIONS

Based on the work done by this study, the following conclusions and recommendations are made:

1. The methods developed in this study allow accurate and rapid assessment of fatigue damage in steel superstructures by the use of strain gages, stress-frequency histograms, and the Palmgren-Miner linear damage rule.
2. The effects of increased truck weight and traffic volume are easily incorporated into the histogram-linear damage method.
3. By calculation of a weld detail safety factor described in this report, planning or design engineers can determine the effects of increasing live or dead loads on new or existing bridge designs and the susceptibility of the bridge superstructure to fatigue failure.
4. Bridges typically have stress ranges between 1.0 to 5.5 ksi and those with heavy truck traffic sustain considerably more fatigue damage over a period of 25 years or more. Although increased truck weight is influential by increasing stress ranges in a linear fashion, traffic growth is far more damaging since it particularly affects those stress ranges where the capacity for cumulative damage is limited. Increasing truck weights by 10 percent and with only a 5 percent traffic growth over a 25-year period causes 4.5 times as much fatigue damage when compared to no traffic growth and no weight increase. A 5 percent increase in traffic will result in 3.4 times as many load cycles over a 25-year period of time for each stress range affected.

5. A composite bridge stress range-frequency histogram for the State of Illinois was developed by averaging the stress range spectra of the 15 bridges surveyed. The maximum stress range in the study was found to be 5.5 ksi. Assuming that if this maximum is quite representative of steel bridges in Illinois, most superstructure details are not at serious risk of fatigue damage. However, susceptible welded steel details, such as cover plates on girders, large longitudinal stiffeners, welded diaphragm connection plates, or sharp changes in section or width, are at risk.
6. Welded details and other main load-carrying members which have been seriously degraded by pitting corrosion or crevicing are susceptible to fatigue damage.
7. Reinforced concrete is at risk if the concrete matrix is severely cracked and the rebar is disbonded.
8. Post-tensioned beams are at risk if the strands are seriously fretted or abraded and the cable ducting is subject to frequent moisture ingress.
9. Bridge decks appear to suffer more damage when compared to the superstructure, particularly in climatic regions where freeze-thaw and traffic conditions warrant the use of deicing salts. Few studies have been completed which can quantitatively indicate the simultaneous effects of cyclic loads, frequency, freeze-thaw and intermittent salt application on reinforced concrete. The lack of plasticity in concrete and its permeable nature render it susceptible to cracking in tension and to the intrusion of saline deicing media which corrodes its ductile

reinforcement. When the deck is being used for composite action to increase the moment of inertia in the supporting girders, cracking of a concrete deck and its loss of integrity puts both the deck and the superstructure at additional risk.

10. A 1:1 direct relationship between percent weight increase and percent stress range increase is a reasonable approximation for multi-girder bridges.
11. A direct corollary of this work is the highlighting of the fatigue reliability of steel bridge superstructures. With both heavy traffic and increasing truck weights, steel bridges still exhibit fatigue resistance and durability, even when using some fatigue-prone details. Elimination of these susceptible details by design in new bridges or the retrofitting or modification of existing bridges can restore even greater life beyond 100 years. Then only corrosion and functional obsolescence will render steel bridges susceptible to failure or replacement.
12. Further study is needed to note the effects of corrosion pits on the plasticity and fatigue life of higher-strength structural steels.
13. Further research is warranted regarding the corrosion fatigue of reinforced concrete bridge decks, other types of reinforced concrete members, and the integrity of post-tensioned concrete using ungrouted cable ducting.

REFERENCES

1. Standard Specifications for Highway Bridges. (1989) American Association of State Highway and Transportation Officials, Washington, D.C., 14th edition.

2. Structural Welding Code/Steel (D1.1). (1984) American Welding Society, Miami, Florida.

3. Moses, F., Schilling, C., and Rajin, K. (November 1987). "Fatigue Evaluation Procedures for Steel Bridges." NCHRP Report 299, Transportation Research Board, Washington, D.C.

4. Munse, W., Wilbur, T., Tellalian, M., Nicoll, K., and Wilson, K. (1983). "Fatigue Characterization of Fabricated Ship Details for Design." Ship Structure Committee, SSC-318, Washington, D.C.

5. Nagaraja Rao, N., Esatuar, F., and Tall, L. (1964). "Residual Stresses in Welded Shapes." Welding Journal, 39(3), Research Supplement, pp. 2958-3068.

6. Gurney, T. (March 1977). "Theoretical Analysis of the Influence of Toe Defects on the Fatigue Strength of Filled Welded Joints." The Welding Institute Research Report 32/1977/E, Cabridge, England.

7. Screm, G., et. al (March 1975). "Effect of Weld Defects In Reducing the Fatigue Strength of Welded Joints." Allumino, 44(3)

8. Harrison, J. (March 1972). "Basis for a Proposed Acceptance Standard for Weld Defects, Part 1: Porosity." Metal Construction and British Welding Journal. 4(3).

9. Frost, N., Marsh, K., and Pook, L. (1974). Metal Fatigue, Oxford University Press, London.

10. Paris, P., Bucci, R., Wessel, E., Clark, W., and Mager, T. (1972) Stress Analysis and Growth of Cracks, ASTM STP 513, Part I.

11. Fuchs, H., and Stephens, R. (1980). Metal Fatigue in Engineering, McGraw Hill, New York, pp. 72-75.

12. Lawrence, F. (1980) "Predicted Influence of Weld Residual Stresses on Fatigue Crack Initiation." Residual Stress for Designers and Metallurgists, American Society for Metals, Metals Park, Ohio, pp. 105-117.

13. Maddox, S. (1982). "Improving the Fatigue Lives of Fillet Welds by Shot Peening." International Association for Bridge and Structural Engineering, Lousanne, Switzerland.

14. Reemsnyder, H. (1978). "Development and Application of Fatigue Data for Structural Steel Weldments." Fatigue Testing of Weldments, ASTM STP 648, p. 3.

15. Booth, G. T., and Wylde, J. (1990). "Procedural Considerations Relating to the Fatigue Testing of Steel Weldments," ASTM STP 1058, Fatigue and Fracture Testing of Weldments, Philadelphia, PA.

16. Fisher, J., Yen, B., Wang, D., and Mann, J. (December 1987). "Fatigue and Fracture Evaluation for Rating of Riveted Bridges." NCHRP Report 302, Transportation Research Board, Washington, D.C.

17. Albrecht, P., Shabshab, C., Li, W., and Wright, W. (1990). "Remaining Fatigue Strength of Corroded Steel Beams." International Association for Bridge and Structural Engineering, Lousanne, Switzerland.

18. Okada, K., Okanuna, H., and Sonoda, K. (September 1978). "Fatigue Failure Mechanism of Reinforced Concrete Bridge Deck Slabs." Bridge Engineering, Vol. 1, Transportation Research Record 664, Transportation Research Board, Washington, D.C.

19. Hodgkiess, T., Arthur, P., and Earl, J. (July 1984). "Corrosion Fatigue of Reinforced Concrete in Seawater." Materials Performance, 23(7), pp. 27-31.

20. Barsom, J. and Rolfe, S. (1987). Fracture and Fatigue Control in Structures. Second Edition, Prentice-Hall, Inc., Englewood Cliffs, NJ, p. 445.

21. Collins, J.A. (1981) Failure of Materials in Mechanical Design, John Wiley, New York, pp. 241-243.